MDPI

Review

Recent Advances in Dielectric Properties-Based Soil Water Content Measurements

Mukhtar Iderawumi Abdulraheem [1,2,3], Hongjun Chen [1,2,3], Linze Li [1,2,3], Abiodun Yusuff Moshood [1,2,3], Wei Zhang [1,2,3], Yani Xiong [1,2,3], Yanyan Zhang [1], Lateef Bamidele Taiwo [4], Aitazaz A. Farooque [5,6] and Jiandong Hu [1,2,3,*]

1   Department of Electrical Engineering, Henan Agricultural University, Zhengzhou 450002, China; abdulraheem@stu.henau.edu.cn or m.iderawumi@gmail.com (M.I.A.); hongjun5555@163.com (H.C.); lilinze@henau.edu.cn (L.L.); yusufbinmasud01@stu.henau.edu.cn (A.Y.M.); zw@henau.edu.cn (W.Z.); xiongyani888@163.com (Y.X.); zyanyan0923@henau.edu.cn (Y.Z.)
2   Henan International Joint Laboratory of Laser Technology in Agriculture Science, Zhengzhou 450002, China
3   State Key Laboratory of Wheat and Maize Crop Science, Zhengzhou 450002, China
4   Institute of Agricultural Research & Training, Obafemi Awolowo University, Moor Plantation, Ibadan P.M.B. 5029, Nigeria; lbtaiwo@oau-ife.edu.ng
5   Faculty of Sustainable Design Engineering, University of Prince Edward Island, Charlottetown, PE C1A 4P3, Canada; afarooque@upei.ca
6   Canadian Centre for Climate Change and Adaptation, University of Prince Edward Island, St Peter's Bay, PE C1A 4P3, Canada
*   Correspondence: jdhu@henau.edu.cn; Tel.: +86-13-3937-06339

Abstract: Dielectric properties are crucial in understanding the behavior of water within soil, particularly the soil water content (SWC), as they measure a material's ability to store an electric charge and are influenced by water and other minerals in the soil. However, a comprehensive review paper is needed that synthesizes the latest developments in this field, identifies the key challenges and limitations, and outlines future research directions. In addition, various factors, such as soil salinity, temperature, texture, probing space, installation gap, density, clay content, sampling volume, and environmental factors, influence the measurement of the dielectric permittivity of the soil. Therefore, this review aims to address the research gap by critically analyzing the current state-of-the-art dielectric properties-based methods for SWC measurements. The motivation for this review is the increasing importance of precise SWC data for various applications such as agriculture, environmental monitoring, and hydrological studies. We examine time domain reflectometry (TDR), frequency domain reflectometry (FDR), ground-penetrating radar (GPR), remote sensing (RS), and capacitance, which are accurate and cost-effective, enabling real-time water resource management and soil health understanding through measuring the travel time of electromagnetic waves in soil and the reflection coefficient of these waves. SWC can be estimated using various approaches, such as TDR, FDR, GPR, and microwave-based techniques. These methods are made possible by increasing the dielectric permittivity and loss factor with SWC. The available dielectric properties are further synthesized on the basis of mathematical models relating apparent permittivity to water content, providing an updated understanding of their development, applications, and monitoring. It also analyzes recent mathematical calibration models, applications, algorithms, challenges, and trends in dielectric permittivity methods for estimating SWC. By consolidating recent advances and highlighting the remaining challenges, this review article aims to guide researchers and practitioners toward more effective strategies for SWC measurements.

Keywords: dielectric properties; soil water content (SWC); electromagnetic energy; soil properties; capacitance; remote sensors

1. Introduction

To efficiently manipulate irrigation systems, agronomists and farmers must collect quantitative data that approximate the variability of soil water content (SWC) on spatial and temporal scales [1–3]. SWC measurement has become an important component of geotechnical analysis, such as in agriculture for irrigation and crop quality [4], in hydrology to determine the rate and amount of soil water movement, and in forests to derive various information about soil water storage capacity. Moreover, due to its link with soil porosities, SWC has an impact on porosity parameters [5]. On the contrary, differences in soil texture and topography cause huge geographical and temporal fluctuations in SWC measurements because soil dielectric permittivity is related to texture (silt, clay, or sand), bulk density, volume particle density (typically 2.6 g/cm^3), soil water content, ambient temperature, and measured frequency [6–8].

The dielectric properties are crucial in understanding the behavior of water within the soil, particularly SWC, since they measure a material's ability to store an electric charge and are influenced by water and other minerals in the soil [9–11]. The water content within the soil significantly influences its dielectric behavior, affecting processes such as plant growth, soil salinity, and nutrient availability [10,12]. In the soil, water can form dipoles, resulting in the storage of electrical energy and increasing the dielectric permittivity. The dissipation factor, another important dielectric property, represents energy loss due to various mechanisms [10,11,13]. As the water content increases, the dissipation factor decreases, indicating less energy loss in the soil [14,15]. Time-domain reflectometry (TDR), frequency-domain reflectometry (FDR), and remote sensing (RS) can all benefit from understanding the link between dielectric characteristics and SWC measurement [12,16,17]. Additionally, the dielectric properties of SWC can be estimated at a distance with remote sensing to maintain optimal conditions for plant growth and development [14,15,18,19]. In irrigation management, dielectric properties can optimize irrigation schedules for crops, conserve water, and reduce the risk of overwatering, which can lead to root rot and nutrient leaching [9].

Many methods have been devised to calculate the SWC from direct or indirect measurements of soil samples. Most SWC sensors use soil dielectric permittivity because it is a crucial parameter in determining SWC due to the difference in relative dielectric permittivity between dry soil and water [10,20]. Due to their reliance on frequency or time, which is connected to the SWC, methods such as FDR and TDR are commonly used, and provide soil-specific calibration with an accuracy of around 0.03 (m^{3}m^{-3}) [10]. TDR involves inserting a probe into the soil, sending an electrical pulse, and determining the time it takes for the pulse to return to the surface, while FDR uses multiple frequencies for more accurate measurements. These measurements can help improve our understanding of soil water dynamics and contribute to more effective and sustainable land management practices [21].

Dielectric permittivity measurements in the microwave region are often unreliable due to the complexity of soil dielectric behavior [11,22]. These measurements require high precision and time due to various factors that affect soil behavior. Laboratory-prepared samples can disturb soil aggregates, making it difficult to determine their representativeness in the field. Despite this, the interpretation of remote sensing data uses these measurements. Studies have been conducted on the dependence of the dielectric permittivity on several parameters, including bulk density, water content, electrical conductivity, soil type, temperature, and frequency [16,23]. Anbazhagan et al. [24] proposed the dielectric mixing model as the best way to obtain SWC from electric permittivity [25] when penetrating radar was grounded using travel time theory. Electrical conductivities pose a special risk to SWC measurement using dielectric spectroscopy [26].

Microwave-based methods are increasingly used in the characterization of moisture content in materials, offering nondestructive, rapid, and accurate measurements suitable for various industries [27,28]. Microwave radiometry, cavity ring-down spectroscopy (CRDS), dielectric spectroscopy, and TDR are some well-known microwave-based techniques for

characterizing moisture content. Dielectric spectroscopy, which is extremely sensitive to the presence of water molecules, evaluates the dielectric permittivity and loss of a material as a function of frequency and temperature [29,30]. With TDR, an electrical pulse is injected into the material, and the reflected signal is measured as a function of time. When describing the moisture distribution of heterogeneous materials, such as soils, wood, and composite materials, CRDS is especially helpful. CRDS involves confining a gas sample within a high-finesse optical cavity and monitoring the exponential decay of light transmitted through the cavity. Water vapor concentrations in air, combustion gases, and industrial process streams have all been effectively measured with CRDS. However, microwave radiometry uses the thermal emission of a material to calculate and monitor the intensity of microwave radiation, which is strongly influenced by the moisture content [27,31]. Various methods have different benefits and drawbacks, depending on the particular material and application. Microwave-based techniques are expected to proliferate in industries that need precise and quick moisture content characterization as technology develops.

The physical characteristics of the soil, which are the most crucial indicators in precision agriculture, are significantly impacted by SWC [4]. Numerous empirical and theoretical models have been presented to assess how SWC and dielectric characteristics relate to each other. The types, textures, wilting points, and transition water content at two frequencies are compiled in Table 1. The dielectric characteristics of identical soil samples are displayed at three frequencies in Table 2 [32,33].

Table 1. Various types of soil are used to measure the dielectric permittivity as a function of water content [32,34].

No	Soil Type	Texture (in Percent)			Wilting Point (cm^3/cm^3)	Transition Water Content (cm^3/cm^3)	Real Part of the Complex Dielectric Permittivity	Imaginary Part of Dielectric Permittivity
		Sand	Silt	Clay				
1	Harlingen clay	2.0	37.0	61.0	0.358	0.31	0.30	0
2	Yuma sand	100.0	0	0	0.004	0.17	0.50	0
3	Eufaula fine sand	90.0	7.0	3.0	0.024	0.16	0.50	0
4	Dougherty fine sand	82.0	14.0	4.0	0.34	0.17	0.50	0
5	Minco very fine sand	70.0	22.0	8.0	0.051	0.17	0.50	0
6	Chinkasha loam	58.0	28.0	14.0	0.098	0.22	0.40	8
7	Open street silt	22.0	70.0	8.0	0.092	0.23	0.50	8
8	Zanies loam	48.0	36.0	16.0	0.114	0.22	0.40	8
9	Collinville loam	45.0	39.0	16.0	0.115	0.23	0.40	8
10	Kirkland silt loam	26.0	56.0	18.0	0.137	0.20	0.40	8
11	Vernon clay loam	16.0	56.0	22.0	0.192	0.28	0.45	26
12	Tabler silt loam	22.0	56.0	22.0	0.159	0.19	0.40	8
13	Long lake clay	6.0	54.0	40.0	0.255	0.26	0.40	26
14	Sand	86.0	7.0	7.0	0.046	0.20	0.40	0
15	Miller clay	3.0	35.0	62.0	0.361	0.33	0.30	20

Table 2. Dielectric properties of soil with different pH values at three frequencies [32].

No	Soil Sample (pH)	ε_r $f_r = 1.88$ GHz	ε_r $f_r = 2.45$ GHz	ε_r $f_r = 5.35$ GHz
1	4.7	3.99	3.90	3.84
2	4.9	3.62	3.43	3.32
3	5.0	3.79	3.53	3.27
4	5.2	3.83	3.75	3.52
5	5.8	3.45	3.76	3.68
6	6.1	3.64	3.47	3.14
7	6.3	3.48	3.55	3.21
8	7.0	3.32	3.72	3.56
9	7.4	3.78	3.80	3.30

The investigation presented in Table 2 above indicates that the real part of the dielectric permittivity ε_r (dielectric constant) with frequency varies for each sample, falling within the range of 3.14 to 3.98. This corresponds to the inverse relationship between frequency and ε_r [32]. However, no consistent pattern is discernible, indicating that the particular value of ε_r is contingent upon the soil sample.

Over the years, various chemical and physical strategies have been investigated to decide on SWC, and a large body of knowledge is now available on the concept with programs [25,35]. Additionally, during the growth phase, there was a significant variation in the monthly trend and vegetation feedback, indicating that soil types had a significant impact on dielectric characteristics. This implies that soil water in sand has dielectric properties similar to those of pure water, which has no dispersion between 50 MHz and 1 GHz [36]. The SWC is dynamic and heterogenetic within spatiotemporal areas due to differences in soil properties, plant type, weather, terrain, and human interruptions. This hinders the development of correct, powerful, non-destructive, and monetary quantification techniques for measuring SWC [36–38]. As soil conductivity increases, resistance decreases and effective capacitance increases. Until the resistance hits $1/\omega C$, when the effective capacitance doubles, this effect is negligible. The probe frequency is lowered as the effective capacitance increases with an additional resistance reduction resulting from the use of TDRs to measure dielectric characteristics. Rainfall, irrigation, and agricultural practices can all exacerbate soil water logging [39], and capacitance sensors can measure the charge time of a capacitor built using a medium to determine the dielectric permittivity of the medium. In FDR, the residual frequency that gauges the amount of water in the soil is found by controlling the oscillator frequency [23].

Soil dielectric permittivity models use SWC, compactness, hardness, structures, and quality indicators to find relationships between the dielectric permittivity and water content [40]. However, sensitivity analysis and calibration models are rarely documented, restricting their use in soil remediation, agricultural soil ecological monitoring, and environmental geo-technology. These models examine the plant nutrient content, soil profile changes, soil thermal capacity, and water resources using dielectric permittivity and physicochemical factors such as salinity, temperature, and water content.

Over the years, several mathematical models have been constructed, but it is still unknown how accurate and comprehensive they are. For most soils, the Topp et al. [41] model was thought to be appropriate; however, for fine-textured soils containing layered clay minerals, different functions are required. There has been variation in the robustness, precision, and usefulness of other models. It is important to gather and categorize mathematical models of TDR because previous research has focused on restricted numbers and kinds of them [17,42]. The effectiveness of TDR mathematical models in predicting soil water content has also been reported in earlier research; however, these studies only examined a small number of models and soils [11,42]. This review aims to synthesize available dielectric-property-based mathematical models relating apparent permittivity to water content, providing an updated understanding of their development, applications, and monitoring.

In this paper, we investigate the basic principles and recent developments in SWC assessments based on dielectric characteristics and how they relate to the water content of soil using capacitance sensors, FDR, GPR, and TDR. Along with discussing the dielectric models for SWC measurements, we examine all related equations of the dielectric permittivity models and present results from various experiments in the measurement of SWC using dielectric properties. We further extensively discuss the application of dielectric models in SWC and present some TDR mathematical models used for dielectric permittivity based on SWC as well as methodological classifications for GPR-based SWC measurement. Finally, we substantiate our findings by examining the applications and configurations of dielectric sensors, their challenges and prospects, and trends in the use of dielectric properties for SWC measurement.

2. Dielectric Models for Soil Water Content Measurements

Due to soil–water interactions, modeling wet soil parameters requires calibration for different soil types [43,44]. The most accurate method is direct field calibration of the petro-physical model, although it is rarely used and necessitates labor-intensive auxiliary measurements [43]. Dielectric measurements are the foundation for the operation of many field soil water content sensors, both experimental and commercial [45,46]. Their range of operation covers several MHz to several GHz, depending on the particular measuring technique and kind of sensor.

Diffusion, volume mixing, and empirical models are the three types of soil dielectric models. Empirical models are used to study the relationship between the dielectric permittivity and the volume of water content for various types of soil [47–49]. The mixing models take into account the dielectric permittivity and the percentage of volume of the solid, liquid, and gas phases of soil [50]. Rayleigh, linear, and root mean square models are examples of representative models [38,51,52]. Diffusion models describe the soil as a homogeneous four-phase mixture using depolarization factors to capture the microscopic effects of continuous and scattered phases [47].

The accuracy of water content estimates can be improved by designing these sensors to match the compositions, textures, and capacities for retaining moisture [10]. In order to ensure accurate measurements accounting for variations or discrepancies in sensor data, effective calibration techniques are also essential [53]. It should be noted that frequent calibration adjustments and checks further improve the accuracy of sensor readings [29,54]. Additionally, to minimize errors associated with generic sensors and provide reliable data for well-informed decision making in agricultural and environmental applications, an efficient strategy for precise water content estimates can be established by combining various sensors tailored for particular soil types with rigorous calibration procedures.

Table 3 shows a summary of the models based on dielectric properties for SWC. Although the TDR technique describes a close relationship between dielectric properties and SWC, actual experiments show that soil environments influence the measurement results [55]. Topp's relation allows the derivation of the values of dielectric properties of soil from known water content profiles [56].

This empirical model was created using TDR between 1 MHz and 1 GHz to measure ε_r for numerous mineral soils. It is written as follows:

$$\varepsilon_r = 3.03 + 155.3\theta - 76.6\theta^3 \tag{1}$$

where ε_r is the dielectric properties (dielectric permittivity) and θ is the volumetric water content of the soil. They also stated the following inverse relation:

$$\theta_v = -2.38 \times 10^{-2} \times \varepsilon_r + 5.5 \times 10^{-4} \times \varepsilon_r + 4.3 \times 10^{-6} \times \varepsilon_r \tag{2}$$

Soil containing more water or organic matter requires a different calibration:

$$\varepsilon_r = 1.40\theta + 135\theta^2 - 55.3\theta^3 \tag{3}$$

The tools for measuring plant water stress depend on the characteristics and use of the soil. Given the energy plants use to draw water from the soil, soil suction may be a more accurate measure than volumetric water content (VWC). Given the variations in sensor response times, a proper sampling frequency is essential. The ideal method may also depend on the physical characteristics of the soil, such as its texture and its capacity to swell or contract. For this reason, GWC is usually used to increase calibrations and validate readings of virtually all VWC measurements, whether in situ or remotely. If there is a dielectric sensor, there might be a way to transform electromagnetic field observations into SWC.

Radio frequency modulations measure SWC, which influences dielectric permittivity, itself used to measure energy storage in the soil. Energy loss is represented by the

imaginary component, while energy storage is represented by the real component. All electromagnetic soil sensors rely on true dielectric permittivity measurements, which are closely correlated with variations in water content [20]. The use of the imaginary component allows for the estimation of accurate electrical conductivity in the 1 to 75 MHz range. Capacitance, measured in farads, is the electrical charge storage unit connected to the actual component. Other factors, such as bulk density and porosity, also have an impact on some of the equations that relate dielectric permittivity to soil water content. Using data from prior studies [9,20,57,58] and the idea of combining models [59], the following equations were presented:

$$\varepsilon = \theta\left(\varepsilon_i + (\varepsilon_w + \varepsilon_i)\frac{\theta}{\theta_t}Y\right) + (\mathfrak{y} - \theta)\varepsilon_a + (1+\mathfrak{y})\varepsilon_r \tag{4}$$

This equation is used for $\theta < \theta_t$, while for $\theta > \theta_t$, the following equation is used:

$$\varepsilon = \theta_t(\varepsilon_i + (\varepsilon_w + \varepsilon_i)Y) + (\theta - \theta_t)\varepsilon_w + (\mathfrak{y} - \theta)\varepsilon_a + (1 - \mathfrak{y})\varepsilon_r \tag{5}$$

where ε_i is the dielectric properties of ice, ε_w = the dielectric properties of water, ε_a = dielectric properties of the air, and ε_r is the dielectric properties of rock (i.e., $\varepsilon_i = 3.2$, $\varepsilon_w = 80$, and $\varepsilon_a = 1$), while θ_t is the transition moisture (0.16–0.33), $\mathfrak{y}$ is the porosity of soil (0.5), and Y is the fitting parameter (0.3–0.5) [59].

Also, the study by Malicki et al. [60] proposed an empirical model using TDR and 62 soil samples, including mineral, organic, pot, artificial, sea, river and forest litter, to determine the SWC. The results show an uncertainty of 0.03 at a 0.05 increment for minerals and organic components ($\varepsilon < \mathfrak{y} < \varepsilon + 0.05$) in the SWC.

$$\theta = \frac{\sqrt{\varepsilon} - 3.47 + 6.22\mathfrak{y} - 3.82\,\mathfrak{y}^2}{7.01 + 6.89\mathfrak{y} - 7.83\,\mathfrak{y}^2} \tag{6}$$

Another physical model was proposed by Roth et al. [51] with an equation based on the dielectric mixing model, which was tested on various soil types using TDR with an error value of no more than 0.013 cm^{3}cm^{-3} [51], resulting in the following equation:

$$\theta = \left(\frac{\varepsilon^Y - (1 - \mathfrak{y})\,\varepsilon_s^Y - \mathfrak{y}\,\varepsilon_a^Y}{\varepsilon_w^Y - \varepsilon_a^Y}\right); +Y = -1 \tag{7}$$

$$\theta = \left(\frac{\varepsilon^Y - (1 - \mathfrak{y})\,\varepsilon_s^Y - \mathfrak{y}\,\varepsilon_a^Y}{\varepsilon_w^Y - \varepsilon_a^Y}\right); +Y = 1 \tag{8}$$

where three phases in series have $\Upsilon = -1$, while three phases in parallel have $\Upsilon = 1$.

Robinson et al. [61] sought to further provide a unique equation for a coarse-textured, layered soil utilizing TDR and coarse-grained quartz and glass beads.

$$\theta = \mathfrak{y}\left(\frac{\sqrt{\varepsilon} - \sqrt{\varepsilon_{dry}}}{\sqrt{\varepsilon_{sat}} - \sqrt{\varepsilon_{dry}}}\right) \tag{9}$$

where ε_{dry} is the permittivity value for dry soil and ε_{sat} is the same for saturated soils.

In their study, Gardner et al. [62] utilized capacitance measurement to determine SWC, and found it ranging from 1.08 to 1.49; they also used multiple linear regression analysis to fit the data, which can be presented as:

$$\theta = \frac{\sqrt{\varepsilon} - 1.208 - 2.454\rho}{9.93} \tag{10}$$

where ρ is the dry bulk density value ranging from 1.08 to 1.49.

Table 3. Summary of all equations of dielectric permittivity models.

	Equations	Source	Soil Type	Experimental Methods	Properties of Soil Bulk Density (g/cm³)	Particle Density (g/cm³)	Porosity
			Model with one parameter				
1	$\varepsilon_r = 3.03 + 155.3\theta - 76.6\theta^3$						
2	$\theta_v = -2.38 \times 10^{-2} \times \varepsilon_r + 5.5 \times 10^{-4} \times \varepsilon_r + 4.3 \times 10^{-6} \times \varepsilon_r$	[41]	• Organic soil • Mineral soil • Glass beads • Vermiculite	ε: using TDR Tektronik Model 7S12 to perform 18 experiments with different treatments θ: using gravimetric technique	1.04–1.44 0.422 1.08 1.49–1.61	-	-
3	$\varepsilon_r = 1.40\theta + 135\theta^2 - 55.3\theta^3$						
			Model with two parameters				
4	$\varepsilon = \theta\left(\varepsilon_i + (\varepsilon_w + \varepsilon_i)\frac{\theta}{\theta_t}Y\right) + (\eta - \theta)\varepsilon_a + (1 + \eta)\varepsilon_r$	[59]	22 different samples	Modeling using data from other studies	1.1–1.7	2.6–2.75	0.4–0.6
5	$\varepsilon = \theta_t(\varepsilon_i + (\varepsilon_w + \varepsilon_i)Y) + (\theta - \theta_t)\varepsilon_w + (\eta - \theta)\varepsilon_a + (1 - \eta)\varepsilon_r$						
6	$\theta = \frac{\sqrt{\varepsilon} - 3.47 + 6.22\eta - 3.82\eta^2}{7.01 + 6.89\eta - 7.83\eta^2}$	[60]	62 soil samples	TDR CAMI	0.13–1.66	1.06–2.7	0.33–0.95
7	$\theta = \left(\frac{\varepsilon^Y - (1 - \eta)\varepsilon_s^Y - \eta\varepsilon_a^Y}{\varepsilon_w^Y - \varepsilon_a^Y}\right); +Y = -1$	[51]	From 11 different field sites	TDR	-	-	-
8	$\theta = \left(\frac{\varepsilon^Y - (1 - \eta)\varepsilon_s^Y - \eta\varepsilon_a^Y}{\varepsilon_w^Y - \varepsilon_a^Y}\right); +Y = 1$						
9	$\theta = \eta\left(\frac{\sqrt{\varepsilon} - \sqrt{\varepsilon_{dry}}}{\sqrt{\varepsilon_{sat}} - \sqrt{\varepsilon_{dry}}}\right)$	[61]	Quartz grain, coarse grain, sandy soil	TDR Tektronix 1502B	-	-	-
10	$\theta = \frac{\sqrt{\varepsilon} - 1.208 - 2.454\rho}{9.93}$	[62]	Silica materials Brown earths	Capacitance probe (80–150 MHz)	1.24–1.63 1.08–1.49	-	-

Plant growth is allowed in mineral soils using this method if the bulk electrical conductivity value is less than 400 m/m^{-1}. It travels to a probe via a coaxial wire with a 50 Ω resistance [44]. Impedance variations cause the signal to reflect, and the time interval between signal points is examined [41,63,64]. High-accuracy calculations of dielectric characteristics are performed using a well-used calibration. Soil EC (salinity) does not affect the procedure. Figure 1 presents the concept of measuring SWC and electrical conductivity simultaneously, together with the corresponding hardware arrangement.

Based on Figure 1a, a fast-sampling oscilloscope records the first pulse from the generator to the sensor in real time, analyzing the electromagnetic wave travel path and calculating the time distance between reflections. Three reflectograms are created for each scenario, representing voltage as a function of time at the selected feeder point. To assess soil electrical conductivity, the study used two 10 cm long TDR probes that were equipped with an analog-to-digital converter, a digital output temperature sensor, a microcontroller, and a serial interface (Figure 1b). The electrical conductivity of the soil sample was determined using a low-frequency conductivity formula and a voltage drop on a reference resistor. The microcontroller produced a square wave at 100 kHz without polarizing the electrode–soil system, distinguishing between higher frequency TDR signals and lower frequencies [65]. The study also found that the bulk dielectric permittivity (ε_b) decreases when the water content is below θeq (water content value) and increases when the water concentrations are above θeq (Figure 1c–e). The temperature effect is explained by the temperature-induced

exchange of water particles. All soils, except soil 562, show values of bulk dielectric permittivity at 5 °C compared to 55 °C with high water content, with medium-value soils showing the largest difference [65,66].
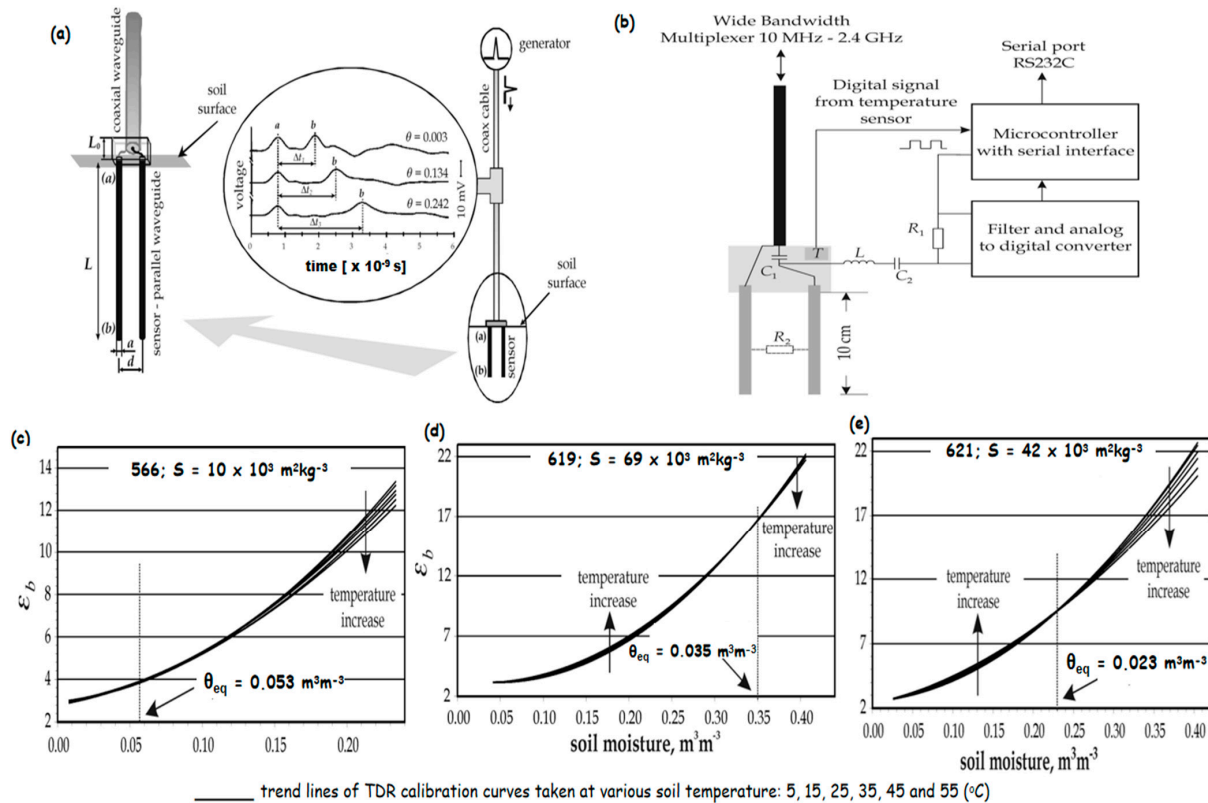

Figure 1. Experimental setups and calibration results for TDR: (**a**) simultaneous measurement of electrical conductivity and SWC (the time distance between two reflections (**a**) and (**b**) are calculated using successive reflections. The reflectograms show voltage changes in soil dielectric permittivity, water content, and electric conductivity. The time (Δt) required for the pulse to cover the double length of metal rods increases with soil dielectric permittivity, resulting in a decrease in pulse amplitude); (**b**) a TDR probe, equipped with electronics, is used to monitor soil temperature and electrical conductivity; (**c**–**e**) TDR calibration curves for three different soil temperatures, where S stands for soil specific surface area and θeq for equilibrium moisture, which accounts for temperature variations [65].

Many variables, such as temperature, salinity, density, and clay content in the case of SWC dielectric sensors, can affect how accurately SWC is measured [12,16]. These variables impact the soil's dielectric permittivity spectrum, as do dielectric dispersion, bound water relaxation, and interphase events [44,67,68]. Consequently, low-frequency device manufacturers frequently offer several calibrations that are suitable for different types of soil, typically distinguishing between mineral and organic soils or focusing on soil texture [69–71]. However, the user can also perform customized calibrations based on the experimental procedures or layout. Park et al. [58] revealed that SWC and the bound water and moisture content, influenced by soil particle composition, affect the dielectric permittivity of the soil. Although TDR and GPR use temperature and texture data to determine refractive index, effective dielectric permittivity, and soil water content, remote sensing assesses brightness temperature (Figure 2a,b). Our study uses laboratory experiments and compares the results with widely used models, validating new approaches in the C band (Figure 2c–e). A logarithmic model is developed to consider the composition of the mesoscopic particles and the bound water content, enhancing the accuracy of calculating the dielectric permittivity of cohesive soils.
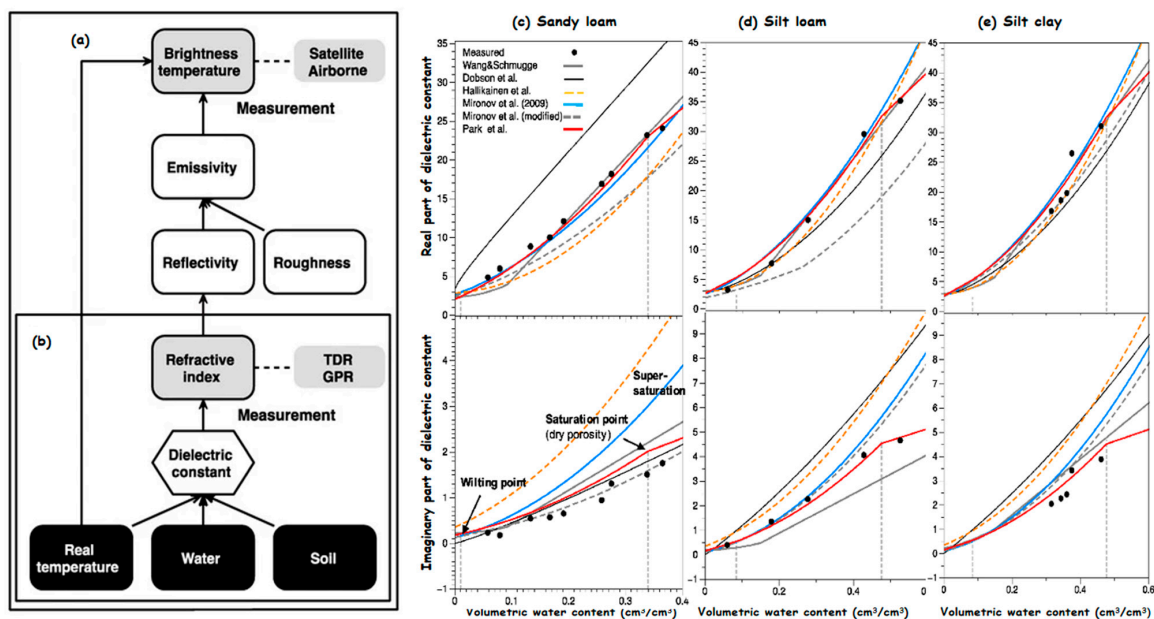
Figure 2. Dielectric constant of the moist soil experiment: (**a**) TDR and GPR sensing setup, (**b**) dielectric constant connection between targeted soil properties and the estimated sensors parameters, (**c**) sandy loam soil of the C band at 5 GHz, (**d**) silt loam at 4 GHz, and (**e**) silt clay at 6 GHz [58].

Not all soil types can be accurately estimated by factory-generic calibrations for SWC sensors, especially those that rely on dielectric permittivity sensing [10]. This study revealed that high-electric conductivity soils have a greater relative inaccuracy in SWC due to the spatial heterogeneity of farmland soils, and laboratory calibration is required. Accurate estimations with 0.05 m^{3}m^{-3} errors are possible at certain locations thanks to soil-specific calibration. Therefore, it is recommended to try to verify the accuracy of the SWC using factory-calibrated commercial sensors before conducting studies on extractable soil water, microbial processes, greenhouse gas fluxes, and spatial variability.

According to Xu et al. [47], the fundamental structure of the soil is affected by the relative dielectric permittivity, which increases with increasing water content (Figure 3a). With an increase in the water content, free water also becomes more polarized, increasing the dielectric permittivity (Figure 3b). The dielectric properties of the soil particles are also influenced by their compaction, since the dry density of the soil influences the spacing of the particles. The dry density also increases the contact area between the soil particles (Figure 3c,d). Large pores and a low dielectric permittivity characterize laterite, which has significant water absorption. Pore water and water film thickness are impacted by the dielectric permittivity, which rises with temperature and water content. Because temperature enhances the thermal movement of water molecules, altering density, viscosity, and polarizability, it has a substantial impact on the dielectric characteristics of the soil. The polarization ability of soil pore water accelerates as temperature rises due to an increase in the relative dielectric permittivity (Figure 3e,f). At a dry density of 1.15 g/cm^{-3}, this growth continues, particularly when the water content is greater than 28% (Figure 3e). At 15 °C in particular, the relative dielectric permittivity increases with temperature (Figure 3f).

According to a study by [38], there are variations in the data obtained from five temperature probes due to the various locations and refrigeration effects. The dielectric permittivity is found to alter with temperature and may be classified into linear and non-linear stages (Figure 4b). The use of five probes improves the accuracy of soil sample temperature measurement. According to the study, during freezing, the dielectric permittivity drops linearly with the increase in temperature, whereas at lower temperatures it decreases rapidly and slowly. Volumetric fractions and soil components affect how the soil dielectric permittivity varies. After 10 h, a silty clay sample containing 0.1% K$_2$SO$_4$ stabilized, suggesting a

12 h hold period (Figure 4a). However, a sudden increase in temperature and a significant decrease in the dielectric permittivity were observed due to latent heat release during the transformation of water into ice [72,73].
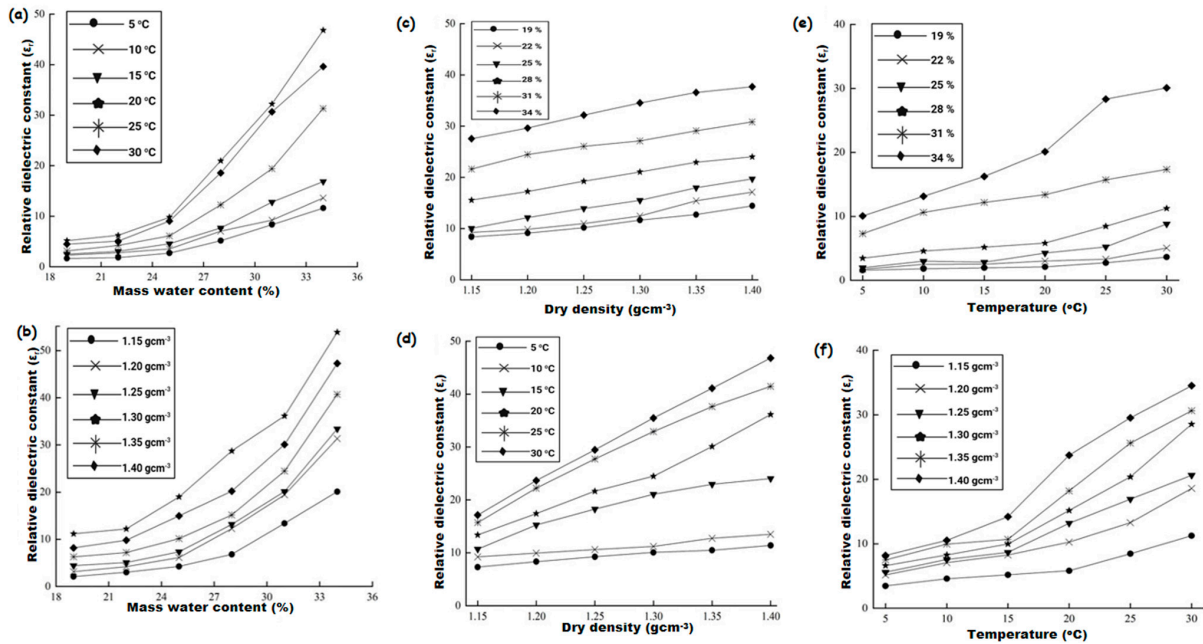

Figure 3. Correlation between the relative dielectric constant and water content at (**a**) ρd = 1.20 gcm^{-3} and (**b**) T = 20 °C; dry density at (**c**) T = 15 °C and (**d**) ω = 28%, and temperature at (**e**) ρd = 1.15 gcm^{-3} and (**f**) ω = 28% [47].

Figure 4. Dielectric constant modeling and measurement. (**a**) Time–temperature dielectric curve of silty clay samples; (**b**) soil temperature changes (the temperature probe coincided with each other in the a–b and g–h stages but show a visible difference in the c–d and e–f stages especially during periods of decreasing temperature); (**c**–**f**) the dielectric constants of silty clay samples are subject to temperature variations and alter with varied water concentrations [38].

3. Remote Sensing Based on Dielectric Properties of Soil Moisture

Soil moisture measurements are typically point measurements acquired using various techniques or embedded sensors such as TDR, FDR, and capacitance [74]. These measurements are considered truthful on the ground because of their close contact with the soil. However, they have limited spatial coverage, necessitating the installation of a large or dense sensor network to monitor large field areas, which can lead to operational and maintenance costs. Improved remote sensing methods for precise soil moisture evaluation have been made possible by developments in dielectric property-based soil water content measurements [28,31,49,75]. This connection facilitates important information on the dynamics of soil moisture, allowing for effective monitoring in wide regions and better decision-making in environmental management, hydrology, and agriculture [76,77]. Based on the dielectric characteristics of the soil, microwave remote sensing techniques determine the moisture content of the soil using electromagnetic radiation in the microwave area [78]. While passive sensors record electromagnetic radiation that is present in the environment, active sensors—such as synthetic aperture radar and ground-penetrating radar—measure electromagnetic radiation that is produced by them.

Understanding soil variability may be greatly aided by RS, particularly in regions with little soil sample availability or difficult topography [28,58]. It is useful for mapping soil characteristics, identifying erosion, and providing high-resolution data on soil parameters such as moisture content and organic carbon concentration [18,19,79]. The ability to see through clouds and vegetation, sensitivity to changes in soil moisture content, and a spatial resolution that can range from a few meters to several kilometers, depending on the sensors used and its altitude above the Earth's surface, are just a few of the advantages that microwave remote sensing has over other methods [75,80,81]. This makes it possible to accurately estimate soil moisture content, even in heavily forested or overcast areas. However, there are several challenges and drawbacks to remote soil moisture detection using dielectric characteristics. For example, it is challenging to create precise models because of the intricate link between soil moisture content and dielectric permittivity. The dielectric permittivity of the soil can be influenced by several factors, such as salinity, temperature, and texture, which can result in inaccurate estimations of soil moisture [17,82]. Due to the attenuation of electromagnetic radiation, the penetration depth of remote sensing methods is restricted, and their spatial resolution might not be adequate for applications that require precise information on small-scale variations in soil moisture content.

The most recent databases, modeling strategies, and ground, near-surface, and satellite remote sensing techniques have been created to quantify surface, near-surface, and root zone soil moisture at different temporal and geographical resolutions [78,83,84]. Spatial soil moisture networks and spatiotemporal SM data are being used more and more to increase our knowledge of hydrological processes, identify trends in the hydrological cycle, test hydrological models, define spatial soil moisture dynamics, and validate satellite RS observations [78,85,86]. However, disparities in the scaling between in situ measurements and satellite sensor resolution, as well as disconnects between the detecting depth of ground and distant sensors, pose difficulties for the validation testing of coarse-scale SM products. Although there are increasing numbers of soil moisture networks in situ, they are not always indicative of the broader surrounding region.

Furthermore, studies have demonstrated the possibility of employing optical and thermal satellite measurements to estimate soil moisture at a high spatial resolution, such as the study of Alexandridis et al. [87], who estimated root zone soil moisture using straightforward ancillary data and energy balance fluxes. The variation in precision was explained by factors such as the types of land cover, the class of soil texture, the time difference between the data sets, and the presence of rain events. With an eight-day time step and a spatial resolution of 250 m, the approach can estimate SM maps at the catchment scale. The possibility of employing optical and thermal band data to estimate soil moisture is demonstrated by both investigations in which surface soil moisture was obtained to give more information on the fusion of microwaves to acquire soil moisture at spatial and

temporal resolutions. Using GPS sensor readings, Koch et al. [88] created a novel method for capturing soil moisture that is based on changes in GPS signal intensity caused by fluctuations in the soil's dielectric permittivity. The utilization of L-band microwave remote sensing data is the primary benefit of the approach, which makes it appealing for use as validation data for SM products. It also allows for continuous extrapolation at typical locations, in addition to complementing satellite data with high geographical coverage but poor temporal precision. The bulk SM of the top soil layer is measured by GPS antennas positioned at a certain soil depth, making it appropriate for global sensors. Furthermore, Li, et al. [89] introduced the GPR-SWC neural network architecture, which enables the rapid inversion of volumetric SWC at field size via the common offset GPR technique. In terms of temporal depth, the model correctly pinpoints various volumetric SWC borders, with a maximum error of less than 0.10 $cm^3 \times cm^{-3}$. Furthermore, the expected values of the soil sample and field values exhibit minimal variation, which is in line with the general trend of changing TDR detection levels. Using farm GPR data, the study reveals that GPR-SWC can invert the soil's water content.

Additionally, Torres-Rua [74] estimated surface soil moisture using meteorological data and Landsat 7 using a Bayesian machine learning technique. The study took advantage of the precision and uncertainty associated with conventional methodologies for Landsat vegetation indices and surface energy balance products. Because the relevant vector machine technique is based on statistical modeling, it does not incorporate embedded uncertainty into the suggested soil moisture model. It is recommended to use quality control processes to validate spatial data, particularly for gap filling, spatial evapotranspiration, and component products used in energy balancing. In remote sensing applications, autocorrelation is anticipated in spatial data; however, statistical behavior in the vector learning machine model is related to the surface soil moisture observed. Future research could anticipate spatial evapotranspiration rate and soil water content for irrigation water balancing operating systems, as well as estimating soil moisture at deeper depths. It is necessary to implement procedures to measure and reduce the influence of data sources and model uncertainty on outcomes.

4. Applications of Dielectric Models in Soil Water Content Measurements

With the use of dielectric permittivity measurements, understanding SWC is crucial for many applications in agriculture, hydrology, environmental management, remote sensing, and soil salinity [11]. By examining how water moves through various soil types, scientists may improve their models that forecast floods and droughts. By evaluating the effects of changing land use on the amount of water in the soil, environmental management can guarantee the sustainability and health of ecosystems. RS applications, such as tracking soil water content using satellite data, can enhance climate models and global water cycles [90]. These measures may also be used to determine the salinity of the soil, which is crucial for agriculture and the health of the environment. This allows farmers to make informed decisions about crop selection and irrigation practices [30]. The results of various experiments on measuring SWC using dielectric properties are extensively discussed in Table 4.

Table 4. Results of various experiments in the measurement of SWC using dielectric properties.

Experiment	Objectives/Aim	Findings	References
Soil's specific features and calibration	Focused on the FDR sensors on their factory calibration	• Highlights the need for calibration and enhances accuracy of SWC determinations in clayed soil.	[10]
Calibration procedure for electromagnetic SWC sensors	To demonstrate the recent and effective calibration methods for low-cost EM sensors	• Sensor-specific calibration increases accuracy • Quickly completes large-scale calibration. • Minimizes errors and requires less work.	[53]

Table 4. *Cont.*

Experiment	Objectives/Aim	Findings	References
Laterite's dielectric characteristics and constant model	To examine the mechanical and physical aspects of in situ laterite dielectric properties	• Laterite dielectric permittivity increases with temperature. • Contributes to dry density and influenced by water content.	[47]
Measurement and modelling of the dielectric permittivity of soil	To suggest, locate, and demonstrate fresh approaches to determining the dielectric permittivity during freezing	• Linear and nonlinear trends. • Higher values during freezing/thawing. • Variations based on soil water content.	[38]
Dielectric analysis models for measurement of SWC	To presents a normalization-based calibration model.	• Estimates water content in each layer during soil infiltration.	[9]
Saturated prediction model using TDR	To suggest the level of soil's saturation with different control criterion for compaction quality	• TDR predicts saturation with $\pm 5\%$ deviance uses the proper model. • Predicts 0.01–0.93 $cm^3 cm^{-3}$ saturation ratio ranges.	[91]
Calibration of the dielectric permittivity model for agricultural soils	To investigates using three pre-established dielectric permittivity models	• The study introduced structural bias, variated with model structure with unchanged porosities.	[43]
Dielectric models for estimating SWC	Examining the link between soil dielectric permittivity, volumetric water content, and dielectric permittivity	• Linear correlations found, models with two segments and shared breakpoint better fit silty and sandy loam textures.	[12]
Mixing models describing dielectric dispersion	To study the dielectric response in the frequency domain of clay minerals and clayey soils	• Novel typologies for the retention of soil water that can be used in sensor design are presented.	[92]
Modeling and measurement of soil dielectric properties	To investigate the dielectric properties at room temperature	• SWC impacted the dielectric characteristics of the soil. • Soils have poorer dielectric qualities than soils with higher water content.	[40]
Dielectric damping and configuration effects on TDR	To investigate the impacts of phase configuration and bound water in four high-surface-area soils	• Sizable volumetric percentages of bound water may require unique soil and probe calibrations.	[93]
Evaluation of the thermal conductivity model	Classification into physical, mixing, normalized, linear, and non-linear regression	• The models performed best in physical, mixing, normalized thermal conductivity, linear and non-linear regression.	[94]
Application of TDR in porous media	To study TDR applications and analyzing waveforms for electrical conductivity and permittivity	• TDR uses snow depth for estimating snow depth, wetting/drying, freezing/thawing fronts. • Electrical conductivity and soil water distribution variability.	[95]
Using TDR probes, field observations of topsoil moisture	To assesses the effectiveness of a novel inverse method to predict water content profiles	• Vertical profiles and water content measurements showed satisfactory agreement. • Some profiles may not find lower water content due to pumice stones.	[96]

<p align="center">**Table 4.** *Cont.*</p>

Experiment	Objectives/Aim	Findings	References
Logarithmic TDR calibration formulas: a physical interpretation	To give an empirical estimate of the solid percentage permittivity in volcanic soils	• The Birchak refractive index model is more suitable for volcanic soils and generally valid for coarse mineral soils.	[97]
TDR field calibration for determining SWC	Examining the dielectric permittivity and gravimetric water content in damaged peatlands	• Identifies soil states. • Improves understanding of soil water regime. • Determines the most appropriate calibration equation for soil water monitoring.	[98]
Temperature-dependent measurement error in TDR determinations of SWC	To compared soil temperature fluctuations in Ka measurement errors with those estimated using a dielectric mixing model	• Significant changes in Ka with temperature in high-water soils. • Absolute water content errors increase linearly with water fraction size.	[99]
Calculating effective approaches for the dielectric permittivity of moist soil	To calculate the effective dielectric permittivity of multiphase soil	• The physical-based model for microwave RS outperforms the popular refractive mixing model. • Identifies a distinct permittivity pattern above the saturation limit. • Increases precision in satellite flood monitoring.	[58]
SWC estimation	To determine the precise dielectric permittivity by calibrating the wave velocity	• GPR wave velocity calibration model reduces sand and clay error by 15.8% and 31.75%. • Demonstrates precision of GPR wave velocity calibration approach.	[100]
A novel soil water sensor that adjusts soil temperature and water content	To adjust and monitor SWC reflectometers for various soil types	• Significant temperature responses across all soils. • Variations in soil water content and type. • Notable calibration variances.	[36]
Soil water remote sensing	To enhance retrieval algorithms and transfer empirical observation at different resolutions	• Upscaling and downscaling functions. • Data assimilation systems for satellite soil water data.	[80]
Dielectric study to quantify the water content of soil	To examine SWC using a new dielectric analysis model	• Suitability of the new model for SWC measurement due to its compatibility with secondary experimental data across soil types.	[101]
Effective field calibration method and model for determining liquid water content	To calculate the amount of uncertainty in the liquid water content	• Connection method in calibration offers better performance and accurate parameter values. • Crucial for regional heterogeneity and prefers excessive data points. • Useful for concurrent measurements and gravimetric samples.	[102]
Soil water measurement by dielectric method	To investigate the dielectric method of measuring SWC and identify sensor values that are differentially influenced by complex dielectric permeability	• Suggests a 0.5–3 GHz frequency range for soil water experiments. • Reduces inaccuracy to 0.014 m^3/m^3 due to interlayer relaxation and soil solution conductivity.	[16]

Table 4. *Cont.*

Experiment	Objectives/Aim	Findings	References
Measurement of SWC with dielectric dispersion frequency	To investigate the possibility of measuring variations in theta using the soil dielectric spectrum	• Study of f (d) methodology is reliable and accurate in dry, high, low soil conditions. • Suitable for theta readings.	[103]
Soil water content retrieval from multispectral remote sensing	To measure SWC with machine learning algorithms and remote sensing	• UAV RS and machine learning for soil water dynamics can successfully describe and predict soil water status.	[82]
Dielectric properties calibration, methods and devices for measuring soil water content	To investigate talc, glass beads, and their combinations at various levels of salinity and water content.	• Calibration curves for soil water measurement minimize data scatter. • Strongly agrees with sand literature and indicates potential applications.	[71]
Distributed fiber-optic sensing for long-range Monitoring	DiTeSt is a laser-based distributed sensing system that utilizes optical scattering within the sensing fiber.	• Enables 300 km pipe-line monitoring. • Crucial for successful instrumentation projects. • Design and manufacture of sensing cables essential.	[104]
Detecting SWC with GPR	Evaluation of the latest advancements in GPR applications in SWC measurement	• Requires significant subsurface contrast in dielectric permittivity. • Requires well-identified, continuous GPR reflections.	[8]
GPR outside the ground for soil water content determination	To examine the connection between SWC and surface characteristics.	• The two most important predictors of surface soil moisture are precipitation and evapotranspiration.	[82]
SWC estimation from remote sensing	To examine recent developments and applications related to SWC estimate from remote sensing	• Expands remotely sensitivity soil moisture application • Enhances SWC recovery accuracy	[105]
Temperature and electrical conductivity effects on an inexpensive SWC	To use a two-sensor array to measure the electrical conductivity sensor used in agricultural fields	• Calibration method's performance demonstrated good performance in soil samples post-fertilization. • Increased electrical conductivity in soil water.	[106]
Soil water retention curves from water content measurements	To develop a new method to estimate soil water retention curves.	• The geometrical relationship estimation of shape parameter α uses three parameters (θs, θr, and m).	[6]
TDR to quantify the SWC and bulk density	Implementation and testing of a novel software for TDR-waveform analysis to measures SWC	• Proposed soil density measurement method offers 1–3% accuracy.	[25]
Monopole antenna-based spectroscopy technique for measuring SWC	To suggest a new approach to measuring soil water that uses frequency scanning	• SWC determination uses linear fitting curve. • Determination coefficient: 0.9834. • Increased SWC leads to lower resonance frequency.	[4]
Determining SWC and bulk density	To determine the TDR calibration slope and effects of electromagnetic waveform on soil salinity	• Salts decrease final voltage values. • Decrease increases with bulk density.	[107]

The experimental setup of GPR is a quick and safe technique used for in-situ measurements of underground media in various fields (Figure 5) [1,108,109]. For data collection, the system makes use of a shielding antenna linked to the ground at 100 MHz [100]. Furthermore, using simulated annealing techniques and genetic algorithms, researchers looked at the experimental water content and the relative dielectric permittivity (Figure 5a–d).
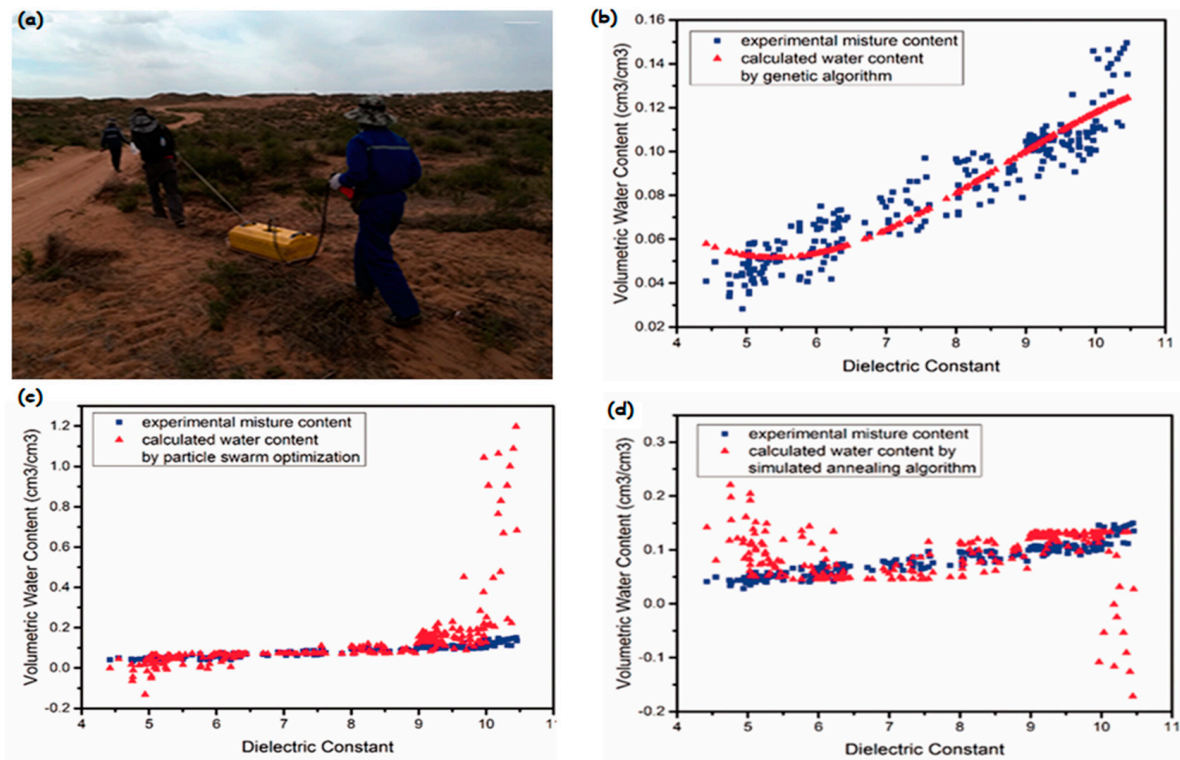

Figure 5. The actual picture of data collection and the intelligent group algorithm optimizes the results: (**a**) GPR detection process, (**b**) results from the genetic algorithm for the sand constants, (**c**) results from the particle swarm optimization for the sand constants, and (**d**) optimized results from the simulated annealing algorithm optimized results for constants of sand [100].

Given that the GPR approach relies on the lifetime of a reflector at a known intensity and that translation procedures rely on a dielectric permittivity evaluation, we must perform determinations and validations [20,23]. The link between soil dielectric permittivity and SWC also varies, which limits its enormous software program. The study in [98] reveals that simple regression models for determining SWC in degraded peatlands are insufficient. The calibration curve provides an acceptable error of 0.04 cm^3cm^{-3}, but the broken-line models are empirical equations that require further research. The study finds that the parameters of the broken-line model correspond to the biodiversity index and bio-indices, which help determine the SWC in degraded peatlands when utilizing the TDR technique. The multivariate approach offers a precise and non-destructive way to assess soft and hard slopes and estimate the state of the surface water content [47]. To increase the precision of measuring the dielectric permittivity of the soil during the freezing and thawing processes, a novel test procedure has been created [38]. To guarantee the right temperature, a 12 h thermostatic time is needed. The findings indicate that the dielectric permittivity of the soil increases as the levels of water, NaCl, and K_2SO_4 increase; however, the new empirical model makes the positive temperature range more significant [38].

To evaluate the uncertainty limit of a dielectric probe to detect the liquid water content in variably frozen soils, the dielectric mixing model has been extended to frozen circumstances [102]. To describe the characteristic curves of soil freezing, this tiny uncertainty limit is helpful, but due to the regional diversity of soil parameters, the field calibration of

dielectric devices presents challenges [71,110]. Both gravimetric measurements and those performed with the same instrument installed are undertaken on many samples to calibrate the probe. Although laborious, this is essential, since an improperly calibrated probe is worse than one that is not. Depending on the application, one may choose to field-calibrate. Amankwah et al. [102] further plotted the mixing models with the most sensitive parameter, α, which influences the intercept of the relationship for the absolute water content, as seen in Figure 6. Nevertheless, ε_s and n are insensitive to variations in water content. Given that the most sensitive parameter is arbitrarily fixed by the empirical model, it can be inferred that α is the least suitable value for varying soil conditions.
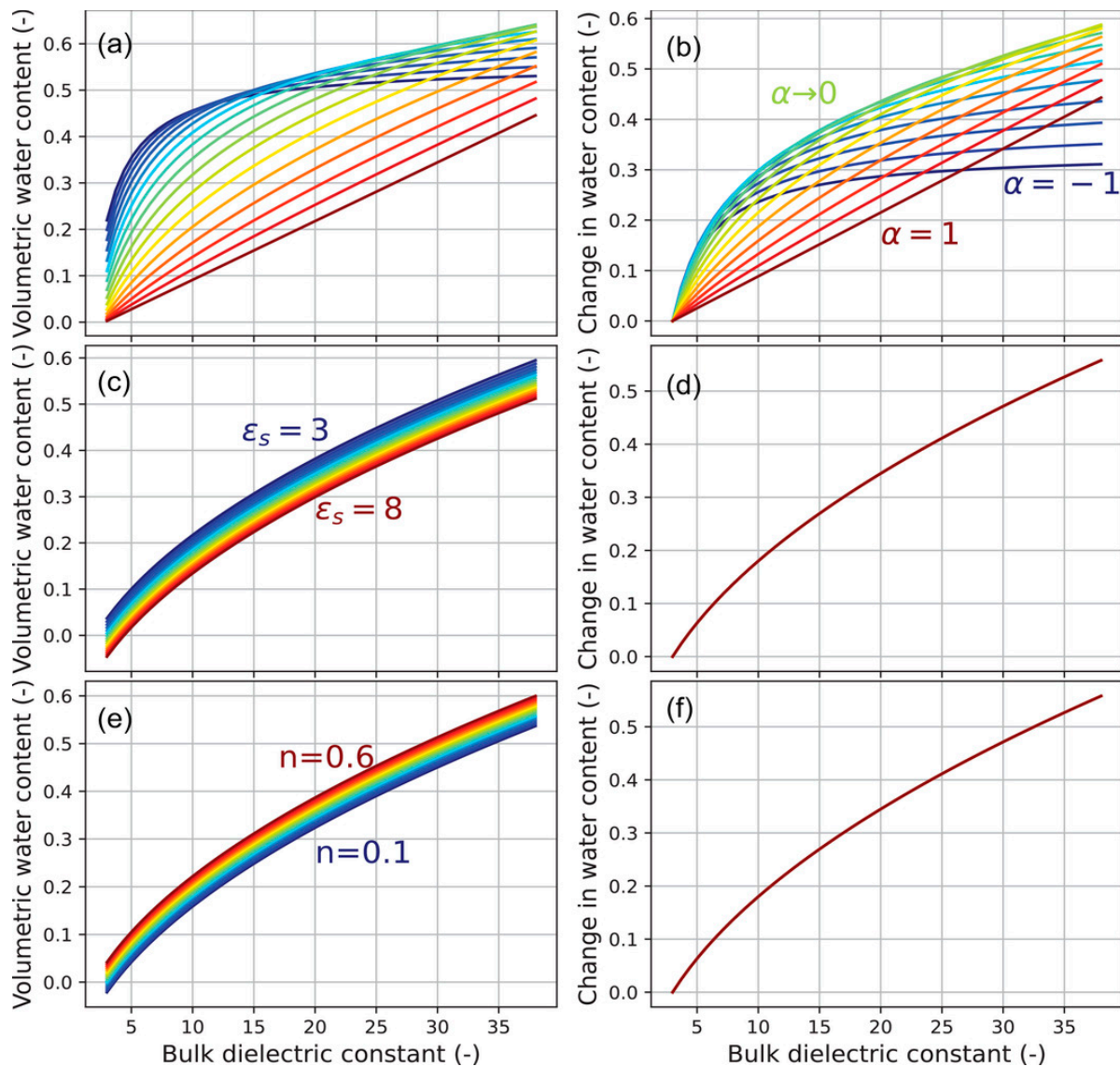

Figure 6. Evaluation of the sensitivity of the mixing model to soil-dependent characteristics. (**a**,**b**) Variations involve adjusting α within -1 and 1; (**c**,**d**) different dielectric constants of the soil between 3 and 8; (**e**,**f**) variation n within 0.1 and 0.6 [102]. (The colors shows the changes in the three unknown parameters, taking realistic upper and lower bound for each parameter).

Researchers have increasingly considered the impact of factors such as bulk density, porosity, temperature, and dielectric permittivity on soil properties [60,62,111]. The most popular model (Table 5) is more versatile and sophisticated and can be applied to soils with varying bulk densities or porosities; other studies have taken into account the effects of water dielectric permittivity and temperature [99].

Table 5. Overview and summary of physical, empirical, and semi-empirical-based TDR mathematical models used for dielectric permittivity based on SWC.

	Model Name	Model Formula	Applicability	References
Empirical models	ZY2016	$\theta_v = \left(\frac{\rho_b\left(-1.4637+\sqrt{K_a}\right)}{22.1373} \right) - 1.4606\sqrt{K_a}$	For soil dry density values larger than 1.3 gcm^{-3}	[111]
	GC2018	$\theta_v = \frac{\sqrt{K_a}+1.208-2.254\rho_b}{9.93}$	Values for the dry bulk density of soil range from 1.08 to 1.49	[62]
	JZ2010	$\theta_v = 0.1228\sqrt{K_a} - 0.1322\rho_b - 0.0152$	All types of soils	[112]
	MM1996	$\theta_v = \frac{\sqrt{K_a}-0.63-0.62\rho_b}{8.04}$	Organic and minerals soils	[60]
	WW2014	$\theta_v = \frac{\sqrt{K_a}+0.4365-1.357\rho_b}{9.566}$	Clay soil	[113]
	SW2020-1	$\theta_v = \frac{\sqrt{K_a}-0.573-0.582\rho_b}{7.755+0.792\rho_b}$	All soil types	[114]
	SW2020-2	$\theta_v = \frac{\sqrt{K_a}+1.177n-2.177}{7.676}$	All soil types	[114]
	SD1995	$\theta_v = \frac{\rho_b}{\rho_w}\frac{1}{b}\left(\frac{\rho_b}{\rho_d}\sqrt{K_a} - a \right)$	All soils types	[115]
	PS2015	$\theta_v = \left(\sqrt{K_a} - \frac{T_s}{T_a} \right)/\left(\sqrt{\varepsilon_\omega} - 1\right)$	Temperature depends on soil water content	[99]
Semi-empirical models	GT2018	$\theta_v = 0.2335 + 0.01178K_a \; K_a$ $\leq K_{a,tp}0.2335 + 0.01178K_{a,tp}$ $+0.007179(K_a - K_a)0 \; K_a$ $\leq K_{a,tp}$	For peat soil	[98]
	RC2014-1	$\theta_v = \frac{1}{1n\varepsilon_{fw}}1nK_a - \frac{(1-n)1n\varepsilon_s}{1n\varepsilon_{fw}}$	3-phase soils	[97]
	RC2014-2	$\theta_v = \frac{1}{1n\varepsilon_{fw}}1nK_a - \frac{(1-n)1n\varepsilon_s+\theta_{bw}1n\left(\varepsilon_{bw}/\varepsilon_{fw}\right)}{1n\varepsilon_{fw}}$	4-phase soils, subscript b$_w$ indicates bound water	[97]
	FS 1997	$K_a = a_0(n) + a_1(n)\theta_v + a_2(n)\theta_v^2 + a_3(n)\theta_v^3$	3-phase soils	[116]
	PN1995	$K_a^\alpha = 1 - \theta_v + \left(\frac{\rho_b}{\rho_b} \right)\varepsilon_a^\alpha + \theta_v^\beta \varepsilon_w^\alpha$	The bulk and particle densities of the sand and clay fractions S and C are given in the text	[117]
Physical models	DM2019	$\sqrt{\varepsilon_{eff}(T)} =$ $\sqrt{\varepsilon_{sat}}\left(\frac{\theta_v-\theta_{v,a}}{\theta_{sat}-\theta_{v,cr}} \right) + \sqrt{\varepsilon_{unsat}}\left(1 - \frac{\theta_v-\theta_{v,a}}{\theta_{sat}-\theta_{v,cr}} \right)$	The terms saturated, unsaturated, and critical point are used to describe 4-phase mixtures in unfrozen soils	[93]
	RD2005	$\sqrt{\varepsilon_{eff}(T)} = \sqrt{\varepsilon_{sat}}\left(\frac{\theta_v-\theta_{hc}}{\varnothing_e} \right) + \sqrt{\varepsilon_{unsat}}\left(1 - \frac{\theta_v-\theta_{hc}}{\varnothing_e} \right)$	The features of soil water retention and aggregated porosity define the hydraulic critical point in aggregated soils, whereas the permittivity of the saturated and unsaturated aggregate layers is represented by ε_{sat} and ε_{unsat}.	[61]
	HD2013	$\varepsilon_{eff} = \varepsilon_0 + \frac{\frac{1}{3}v(\varepsilon_{eff}-\varepsilon_O)\Sigma_{k=x,y,z}1\frac{na_k}{\varepsilon_o+\frac{1}{3}v\left(\varepsilon_{eff}-\varepsilon_O\right)}}{1-\frac{1}{3}\Sigma_{k=x,y,z}N_k^{(j)}\frac{na_k}{\varepsilon_o+\frac{1}{3}v\left(\varepsilon_{eff}-\varepsilon_o\right)}}$	Confocal model	[95]
	ZM2016	$\varepsilon_{eff} = \frac{1}{3(2_n-\theta_v)}\theta_v\varepsilon_w + (1 - n)\varepsilon_s + (n - \theta_v)\varepsilon_a$	Glass beads and unsaturated soils (3 phase mixtures)	[118]

The study by [92] reveals that the permittivity of clay minerals and clayey soils is significantly influenced by Maxwell–Wagner relaxation processes, which shift the permittivity from the high-frequency to the low-frequency end. The results of the investigation demonstrate the sensitivity of the soil permittivity response, with slight variations producing large variations. This response is influenced by variables such as conductivity, porosity, ECw, and the heuristic parameter. The permittivity dispersion below 100 MHz is approximated using a model that allows substantial interaction between inclusions. In clay soils, Maxwell–Wagner relaxation processes predominate, and the dielectric response is determined by the phase composition and geometry.

The soil permittivity is controlled by the SWC, which is determined by the travel time between an antenna and a reflector target [119]. SWC is measured using GPR, and information about SWC is immediately retrieved from GPR data in the frequency domain using frequency shift algorithms [120]. Some techniques, referred to as "dielectric permittivity methods" begin by measuring the permittivity of the soil (Table 6) and then calculate the SWC by using an empirical equation or on-site calibration to establish the link between the two parameters.

Table 6. Methodological classifications and related references for GPR-based SWC measurements.

Classification of Methods	Configurations of Radar System	Signal Attributes Used in Method	Reference Depth Range of SWC Estimation	Antenna Frequency Used in References (MHz)	References
Reflected wave method	Ground-coupled GPR	Time	Depth of reflector	450; 900 225/450/900	[108]
Ground wave method	Ground-coupled GPR (or surface GPR)	Time	≤30 cm (Penetrating depth of ground wave in soil)	225/450/900	[121]
AEA method	Ground-coupled GPR	Amplitude and Waveform	≤30 cm	250/500	[1,122]
FWI method	--	All attributes of recorded signal	~2 cm	1000~2000	[123]
Frequency shift method	Ground-coupled GPR	Energy and phase etc.	10 cm	600	[2]
Borehole GPR method	Borehole GPR	Time	Maximum distance between receiver and transmitter	100; 250	[119]

When the dielectric permittivity is converted from GPR to volumetric SWC, relationships must be used. Typically, GPR connections are generated via TDR calibration. GPR fills the gap between satellite-based large-scale measurements and sensor-based small-scale observations by combining TDR and GPR [24]. The approach works by analyzing high-frequency electromagnetic waves (3–30 GHz) emitted by the surface soil layer and detecting reflected waves [124]. The rate of attenuation of GPR signals in soil is influenced by the dielectric permittivity of the soil.

The combination of TDR and FDR methods can provide more precise and reliable measurements of SWC because TDR measures the time differences between transmitted and reflected pulses, while FDR measures the phase change and attenuation of the reflected signal [125]. This information is used to determine the distance to the reflection point and the material's dielectric permittivity. Combining TDR and FDR can also improve measurement accuracy by minimizing noise and interference. TDR can also be used to calibrate FDR readings, creating a calibration curve that relates FDR results to soil water content [126,127]. The combination of TDR and FDR technologies in SWC can improve irrigation schedules, reduce water waste, reveal the health and resilience of wetlands,

forests, and other ecosystems, as well as being used to monitor soil moisture levels in dams, levees, and other structures, identifying possible stability issues before they become serious in geotechnical engineering [127].

By measuring the volumetric water content of the soil using the TDR, the study by [128] was able to identify differences within the Wiener and Hashin–Shtrikman limits. The high viscosity of the soil significantly influenced the bound water, leading to high Topp formula values. Table 7 further shows the applications and configurations of dielectric sensors for measuring water content. However, the Looyenga formula, the Maxwell–Garnett model, and the differential effective medium model were found to be more effective. The study suggests that considering the distribution of water and gas in the soil can result in a weighted average of single-phase calculations.

Table 7. Application and configuration of dielectric sensors for water content measurement using TDR.

Configurations				Applications	References
Probe Length (cm)	No of Rod/Probe	Diameter (mm)	Spacing (mm)		
120	2	3.0	30	Measurement of soil and oak stem water content in a lab	[129]
40–45	7	3.0	7	Lab test	[63]
250	3	5	30	GPR and TDR mapping of the depth, density, and layering of dry snow	[9,11]
105, 150, 300	1	3.0	32	Top soil water profile in the field	[96]
480	1	37	-	Obtaining a 3 m depth soil water profile, perfect for high-salinity soil	[128,130]
100	2	2	16	Soil salinity, water and temperature	[131]
200	2	3	50	Field measurement SWC	[37]
110/160	2	3.5/6	20/40	Soil temperature and water content	[132]
98	7	2	15	Complex dielectric permittivity of soil	[58]
99–380	3	3–12	8–57	Field, spatial variability of θ_v	[133]
150	2, 3	4	20	Comparing parallel plates with traditional rods in a field and laboratory test to measure SWC	[134]
150	3–4	4.76	30	Field measurement of θ and EC	[36]

According to mixture theory, the dielectric permittivity increases with the SWC at both positive and negative temperatures [38,135]. A higher water content causes the volumetric proportion of water to increase and the proportion of air at the pores to decrease, so an increase in SWC lowers the dielectric permittivity in negative temperatures [135]. Using data from the immersion technique to estimate the dielectric permittivity of solid materials [93], a method for calibrating mixing models may reduce uncertainty in indirect estimates of bound water permittivity and parameters of bound water permittivity models. A conjecture suggests that the significant slope increase in Andosols after the water content exceeds a threshold value is due to increased dielectric properties (temperature, water content) due to lower frequencies at higher water content, likely due to bulk water polarization attenuation of the incident electromagnetic wave. The combination of TDR measurements and effective frequency estimations to gain a better understanding of electromagnetic properties and the impact of phase configuration on soil structure may also affect broadband electromagnetic wave attenuation.

5. Challenges, Prospects, and Trends in Using Dielectric Properties to Measure SWC

5.1. Challenges

Dielectric properties-based soil water content measurement techniques offer significant advantages over traditional methods. They provide non-destructive, continuous, and rapid measurements of soil water content, making them valuable tools for agriculture, hydrology, and environmental sciences [47,77,103]. However, challenges related to calibration, sensor placement, soil heterogeneity, integration with other technologies, and data analysis need to be addressed to advance this field. The difficulty of measuring water near surfaces, particularly its dielectric behavior, is a significant obstacle to understanding its behavior. New techniques are improving our understanding of water at interfaces [92]. Determining the correlation between soil types and dielectric properties poses a challenge in the calibration and validation of dielectric sensors for SWC monitoring. Furthermore, a complete understanding of the influence of soil mass on the measurement of SWC is lacking in existing studies. There remains concern regarding the validity of widely used dielectric response-based techniques and their applicability to different types of soils and water content. To fully understand how these factors affect SWC measurement and how useful these methods are for precise measurements, more research is required.

By simulating an uncharged silica surface, Kargas et al. [37] discovered that surfaces can impede the ability of water molecules to rotate up to 10 nm away. The orientation of the dipole is changed by the structural arrangement of the confined water, not by electrostatic forces caused by the hydration of ions or negatively charged surfaces [102]. There is still disagreement about whether the drop in the dielectric profile is a reflection of the intrinsic or ionic characteristics of the water. When the solution is confined to spheres or nanotubes, the dielectric value drops due to a variety of molecular causes, such as electrostatic forces, molecule ordering, hydrogen bonding breaking, and water orientation. The characteristics of the surface, whether hydrophilic or hydrophobic, also affect the water structure. It is challenging to determine a general relationship between dielectric properties and SWC in a variety of soil types due to the complexity of soil composition, which includes varying levels of organic matter, mineral content, and pore structure [22]. Furthermore, temperature affects the dielectric characteristics, which can cause errors in SWC measurements. The accuracy of SWC tests based on dielectric characteristics can potentially be affected by high salinity and electrical conductivity levels.

Furthermore, the manufacturer's dielectric equation for a capacitance sensor is usually based on different fixed mineral soils, but the data presented may be derived primarily from highly porous sand, leading to a difference between the factory-calibrated values and real values [136–138]. The problem lies in the difference in bulk density found in different soil types, which inherently can hold more or less water. Calibration for each type of soil texture and bulk density is necessary to avoid misleading and potentially meaningless measurements. Furthermore, the variations between sensors account for a large portion of the measurement errors in soil water content. Instead of calibrating sensors for sensor-to-sensor variation, manufacturers frequently advise calibrating sensors for variations in bulk density and soil texture. This can result in errors in irrigation scheduling, catchment water budgeting, and scientific modeling. It is strongly advised that each sensor be calibrated separately to guarantee perfect precision rather than depending on the sensor-to-sensor variation.

Measurements of the dielectric permittivity could also lead to errors in soil water content sensors because the dielectric characteristics of water, soil, and air are used in these measurements, as well as electromagnetic measurements [3,20]. The calibration and validation of the dielectric sensor must take into account several characteristics, such as soil compaction, texture, and organic matter concentration, which can be difficult to achieve. An additional problem is spatial diversity in the physical and chemical properties of the soil, since the heterogeneity of SWC within a particular area could be missed by a single sensor. Furthermore, the accuracy of SWC measurements may be affected by imperfections in the soil structure that interfere with the electromagnetic field produced by

the dielectric sensors. However, the dielectric permittivity can be impacted by changes in temperature and highly clayed soil. Furthermore, results can be greatly affected by salinity or electrical conductivity, which makes it difficult for inexpensive TDR and capacitance sensors to reliably measure in soils with EC values greater than 1 dS/m. Finally, there might have been a mistake in the sensor calibration process used by the manufacturer. It is not advisable to assume that manufacturers have the necessary equipment or know-how to calibrate their sensors correctly.

5.2. Prospective and Future Trends

The dielectric models used for a dielectric measurement technique such as TDR, FDR, or GPR depend on the desired precision of the user and known field conditions [43]. Geographical and temporal soil porosity information is typically unavailable for field use, but can be obtained for laboratory calibration [129]. Maintaining constant porosity variation between field application and calibration is challenging, so a generalized porosity constant is recommended [43]. However, ambiguity can cause problems for models with high porosity sensitivity, which limits their applicability to agricultural soils with systematic variations in porosity.

Because dielectric characteristics are sensitive to changes in water content, they are used to quantify SWC. This methodology presents several opportunities and future directions for measuring soil moisture because it consists of enhanced precision and accuracy, non-destructive and instantaneous monitoring, incorporation with remote sensing technologies, multi-sensor fusion methodologies, and progressions in sensor design and downsizing. Prospective developments involve the use of machine learning algorithms and data-driven methodologies to construct more resilient calibration models, the integration of heterogeneity components of the soil, and the formulation of validation and standardization procedures. Furthermore, future developments in calibration model refinement will be driven by advances in our understanding of dielectric behavior in heterogeneous soil systems. This involves looking at interactions with soil salinity, temperature impacts, and frequency-dependent effects. To take into account particular environmental conditions and user requirements, application-specific calibration models will also be built. Overall, increased precision, non-destructive monitoring, integration with remote sensing technologies, multi-sensor fusion techniques, advances in sensor design, machine learning applications, a better comprehension of dielectric behavior, and application-specific modeling are all potential uses of dielectric properties for SWC measurement in the future.

A wide range of soil conditions may not be adequately represented by existing TDR mathematical models [139]. Although there are databases for soil physical parameters such as moisture, pressure, and temperature, there are no databases for apparent soil dielectric permittivity [94,140]. It is necessary to have a database containing information on bulk density, pH, electrical conductivity, soil texture, and water content [11,20]. This will enable the evaluation of current TDR mathematical models and improve the understanding of soil properties. SWC is important when analyzing soil water regimes, and the gravimetric approach is the most accurate. Since soil samples must be withdrawn for ongoing monitoring, radioactive technologies such as gamma-ray attenuation and neutron scattering are generally accepted as non-destructive in situ methods for measuring soil water content [17,141]. For effective and accurate functioning, the procedures require proper soil calibration and additional precautions due to environmental and health risks. Other widely used methods include capacitance, FDR, TDR, GPR, and passive microwave approaches [142]. These approaches are simple to operate, but require calibration for each soil and, occasionally, for each sensor, which vary in size, precision, and cost.

Modern inversion techniques provide improved subsurface information, and linked inversion can extract hydraulic parameters from time-lapse SWC data [8,143]. However, these techniques have drawbacks, such as the intricate TDR and GPR operations and their sensitivity to temperature, electrical conductivity, and bulk density [5,55,144,145]. The effectiveness of these sensors is limited by the impacts of dielectric losses in clay and

salinized soils. Once must remove the electrical conductivity of the soil sample before using capacitance sensors for the SWC measurement. When examining the results of the SWC measurements, it is imperative to differentiate between active and reactive components [3,32,73]. It should also be noted that the electrical capacitance-based dielectric permittivity has a strong correlation with the SWC, with an increase in reduction under near-saturation conditions and a low increase in speed when the water content is small. This relationship should be limited to cases where electrical capacitance remains unchanged during measurement, and suggests that the modified model should propose a more extensive suitability and have more fundamental physical meanings than the existing models.

Steady-state dielectric procedures are more accurate, faster, and cheaper than gravimetric approaches [82]. The dielectric data are continuous and can be saved online or transmitted to a computer. Dielectric procedures are popular because they are quick, in situ, non-destructive, and precise [107]. The dielectric properties of water have been used to measure the SWC at high frequencies because the dielectric permittivity is predicted by electromagnetic waves or pulses in the soil. However, more research is needed on down- and up-scaling methodologies and large-scale modeling to achieve valid SWC estimates [129]. Dielectric permittivity-based approaches can accurately and efficiently monitor SWC on a broad scale, and instrumentation improvements, such as multichannel high-speed measurements and 5G network architecture, can facilitate data processing and mathematical analysis [129]. Interpretation approaches require well-defined and continuous reflections that require substantial and spatially continuous subsurface dielectric permittivity contrast. However, the wavelength-based method, which uses existing thermal conductivity models for soil texture and composition, can be used without laboratory calibrations, but has a larger measurement error because of soil type variations, requiring alternative models.

6. Conclusions

In conclusion, this review document explores recent advances in soil water content measurements based on dielectric properties. It discusses various techniques, methods, advantages, limitations, sensor technologies, data processing algorithms, and calibration procedures. The paper emphasizes the importance of understanding dielectric properties and their influence on soil water content determination, providing valuable information to researchers, practitioners, and stakeholders in agriculture, environmental monitoring, and hydrology. The review article serves as a resource to advance knowledge and promote innovation in the measurement of soil water content. Through our findings, it has become clear that technological advancements in dielectric-based soil water content measurements have significantly improved the efficiency and accuracy of SWC monitoring, allowing real-time data collection for agricultural, environmental, and geotechnical applications. In addition, theoretical developments have led to a deeper understanding of the complex interactions between soil properties and dielectric permittivity, allowing for a more precise estimation of soil water content. These findings have identified that advanced modeling techniques and data analysis methods have further enhanced the interpretation of dielectric measurements, facilitating the extraction of valuable information about soil water dynamics and spatial variability. Lastly, these measurements have been instrumental in optimizing irrigation practices, assessing the impact of soil water on crop health, and monitoring water resources in both agricultural and natural ecosystems. More research is needed to improve the accuracy and reliability of soil water content measurements based on dielectric properties, including examining soil variations, integrating advanced data processing techniques, and developing new sensor designs.

Conflicts of Interest: The authors declare that they have no conflicts of interest.

References

1. Algeo, J.; Van Dam, R.L.; Slater, L. Early-Time GPR: A Method to Monitor Spatial Variations in Soil Water Content during Irrigation in Clay Soils. *Vadose Zone J.* **2016**, *15*, 1–9. [CrossRef]
2. Benedetto, A.; Tosti, F.; Ortuani, B.; Giudici, M.; Mele, M. Mapping the spatial variation of soil moisture at the large scale using GPR for pavement applications. *Near Surf. Geophys.* **2015**, *13*, 269–278. [CrossRef]
3. Wan, H.; Qi, H.; Shang, S. Estimating soil water and salt contents from field measurements with time domain reflectometry using machine learning algorithms. *Agric. Water Manag.* **2023**, *285*, 108364. [CrossRef]
4. Li, M.; Jwo, K.-W.; Yi, W. A novel spectroscopy-based method using monopole antenna for measuring soil water content. *Measurement* **2021**, *168*, 108459. [CrossRef]
5. Bao, J.; Hou, Z.; Ray, J.; Huang, M.; Swiler, L.; Ren, H. Soil moisture estimation using tomographic ground penetrating radar in a MCMC–Bayesian framework. *Stoch. Environ. Res. Risk Assess.* **2018**, *32*, 2213–2231. [CrossRef]
6. Fu, Z.; Zhang, X.; Zhang, H.; Li, Y.; Zhou, H.; Zhang, Y. On the Understandings of Dielectric Constant and Its Impacts on the Photovoltaic Efficiency in Organic Solar Cells. *Chin. J. Chem.* **2021**, *39*, 381–390. [CrossRef]
7. Farhat, I.; Farrugia, L.; Bonello, J.; Sammut, C.; Persico, R. Measuring the Dielectric Properties of Soil: A Review and Some Innovative Proposals. In *Instrumentation and Measurement Technologies for Water Cycle Management*; Di Mauro, A., Scozzari, A., Soldovieri, F., Eds.; Springer International Publishing: Cham, Switzerland, 2022; pp. 485–509.
8. Klotzsche, A.; Jonard, F.; Looms, M.C.; van der Kruk, J.; Huisman, J.A. Measuring Soil Water Content with Ground Penetrating Radar: A Decade of Progress. *Vadose Zone J.* **2018**, *17*, 180052. [CrossRef]
9. Mukhlisin, M.; Saputra, A. Dielectric Analysis Model for Measurement of Soil Moisture Water Content Using Electrical Capacitance Volume Tomography. In *Modern Applications of Electrostatics and Dielectrics*; Dengming, X., Krishnaswamy, S., Eds.; IntechOpen: Rijeka, Croatia, 2019.
10. Zawilski, B.M.; Granouillac, F.; Claverie, N.; Lemaire, B.; Brut, A.; Tallec, T. Calculation of soil water content using dielectric-permittivity-based sensors—Benefits of soil-specific calibration. *Geosci. Instrum. Method. Data Syst.* **2023**, *12*, 45–56. [CrossRef]
11. He, H.; Zou, W.; Jones, S.B.; Robinson, D.A.; Horton, R.; Dyck, M.; Filipović, V.; Noborio, K.; Bristow, K.; Gong, Y.; et al. Critical review of the models used to determine soil water content using TDR-measured apparent permittivity. In *Advances in Agronomy*; Sparks, D.L., Ed.; Academic Press: Cambridge, MA, USA, 2023; Volume 182, pp. 169–219.
12. Szypłowska, A.; Lewandowski, A.; Yagihara, S.; Saito, H.; Furuhata, K.; Szerement, J.; Kafarski, M.; Wilczek, A.; Majcher, J.; Woszczyk, A.; et al. Dielectric models for moisture determination of soils with variable organic matter content. *Geoderma* **2021**, *401*, 115288. [CrossRef]
13. Liu, J.; He, T.; Yang, Z.; Peng, S.; Zhu, Y.; Li, H.; Lu, D.; Li, Q.; Feng, Y.; Chen, K.; et al. Insight into the mechanism of nano-TiO2-doped biochar in mitigating cadmium mobility in soil-pak choi system. *Sci. Total Environ.* **2024**, *916*, 169996. [CrossRef]
14. Quan, C.; Jiuli, L.; Zhihua, T.; Jiangyuan, Z.; Yan, L. Study on the relationship between soil moisture and its dielectric constant obtained by space-borne microwave radiometers and scatterometers. *IOP Conf. Ser. Earth Environ. Sci.* **2014**, *17*, 012143. [CrossRef]
15. Zhou, G.; Su, S.; Xu, J.; Tian, Z.; Cao, Q. Bathymetry Retrieval From Spaceborne Multispectral Subsurface Reflectance. *IEEE J. Sel. Top. Appl. Earth Obs. Remote Sens.* **2023**, *16*, 2547–2558. [CrossRef]
16. Bobrov, P.P.; Belyaeva, T.A.; Kroshka, E.S.; Rodionova, O.V. Soil Moisture Measurement by the Dielectric Method. *Eurasian Soil Sci.* **2019**, *52*, 822–833. [CrossRef]
17. Nielsen, C.K.; Thomsen, A.G. Local Calibration of TDR Measurements for Determining Water and Organic Carbon Contents of Peaty Soils. *Soil Syst.* **2023**, *7*, 10. [CrossRef]
18. Abdulraheem, M.I.; Zhang, W.; Li, S.; Moshayedi, A.J.; Farooque, A.A.; Hu, J. Advancement of Remote Sensing for Soil Measurements and Applications: A Comprehensive Review. *Sustainability* **2023**, *15*, 15444. [CrossRef]
19. Quemada, C.; Pérez-Escudero, J.M.; Gonzalo, R.; Ederra, I.; Santesteban, L.G.; Torres, N.; Iriarte, J.C. Remote Sensing for Plant Water Content Monitoring: A Review. *Remote Sens.* **2021**, *13*, 2088. [CrossRef]
20. Rehman, F.; Abouelnaga, H.S.O.; Rehman, F. Estimation of dielectric permittivity, water content, and porosity for environmental engineering and hydrogeological studies using ground penetrating radar, a short review. *Arab. J. Geosci.* **2016**, *9*, 312. [CrossRef]
21. Zhu, G.; Yong, L.; Zhao, X.; Liu, Y.; Zhang, Z.; Xu, Y.; Sun, Z.; Sang, L.; Wang, L. Evaporation, infiltration and storage of soil water in different vegetation zones in the Qilian Mountains: A stable isotope perspective. *Hydrol. Earth Syst. Sci.* **2022**, *26*, 3771–3784. [CrossRef]
22. Dai, H.; Ju, J.; Gui, D.; Zhu, Y.; Ye, M.; Liu, Y.; Cui, J.; Hu, B.X. A two-step Bayesian network-based process sensitivity analysis for complex nitrogen reactive transport modeling. *J. Hydrol.* **2024**, *632*, 130903. [CrossRef]
23. Zhou, L.; Yu, D.; Wang, Z.; Wang, X. Soil Water Content Estimation Using High-Frequency Ground Penetrating Radar. *Water* **2019**, *11*, 1036. [CrossRef]

24. Anbazhagan, P.; Bittelli, M.; Pallepati, R.R.; Mahajan, P. Comparison of soil water content estimation equations using ground penetrating radar. *J. Hydrol.* **2020**, *588*, 125039. [CrossRef]

25. Bittelli, M.; Tomei, F.; Anbazhagan, P.; Pallapati, R.R.; Mahajan, P.; Meisina, C.; Bordoni, M.; Valentino, R. Measurement of soil bulk density and water content with time domain reflectometry: Algorithm implementation and method analysis. *J. Hydrol.* **2021**, *598*, 126389. [CrossRef]

26. Shan, G.; Sun, Y.; Zhou, H.; Schulze Lammers, P.; Grantz, D.A.; Xue, X.; Wang, Z. A horizontal mobile dielectric sensor to assess dynamic soil water content and flows: Direct measurements under drip irrigation compared with HYDRUS-2D model simulation. *Biosyst. Eng.* **2019**, *179*, 13–21. [CrossRef]

27. Piuzzi, E.; Cannazza, G.; Cataldo, A.; De Benedetto, E.; De Giorgi, L.; Frezza, F.; Leucci, G.; Pisa, S.; Pittella, E.; Prontera, S.; et al. A comparative assessment of microwave-based methods for moisture content characterization in stone materials. *Measurement* **2018**, *114*, 493–500. [CrossRef]

28. Huang, J.; Ma, H.; Sedano, F.; Lewis, P.; Liang, S.; Wu, Q.; Su, W.; Zhang, X.; Zhu, D. Evaluation of regional estimates of winter wheat yield by assimilating three remotely sensed reflectance datasets into the coupled WOFOST–PROSAIL model. *Eur. J. Agron.* **2019**, *102*, 1–13. [CrossRef]

29. Mane, S.; Das, N.; Singh, G.; Cosh, M.; Dong, Y. Advancements in dielectric soil moisture sensor Calibration: A comprehensive review of methods and techniques. *Comput. Electron. Agric.* **2024**, *218C*, 108686. [CrossRef]

30. Jiao, Y.; Zhu, G.; Meng, G.; Lu, S.; Qiu, D.; Lin, X.; Li, R.; Wang, Q.; Chen, L.; Zhao, L.; et al. Estimating non-productive water loss in irrigated farmland in arid oasis regions: Based on stable isotope data. *Agric. Water Manag.* **2023**, *289*, 108515. [CrossRef]

31. Bai, B.; Xu, T.; Nie, Q.; Li, P. Temperature-driven migration of heavy metal Pb2+ along with moisture movement in unsaturated soils. *Int. J. Heat Mass Transf.* **2020**, *153*, 119573. [CrossRef]

32. Mohan, R.R.; Paul, B.; Mridula, S.; Mohanan, P. Measurement of Soil Moisture Content at Microwave Frequencies. *Procedia Comput. Sci.* **2015**, *46*, 1238–1245. [CrossRef]

33. Kelleners, T.J.; Verma, A.K. Measured and Modeled Dielectric Properties of Soils at 50 Megahertz. *Soil Sci. Soc. Am. J.* **2010**, *74*, 744–752. [CrossRef]

34. Mo, H.; Wang, G.; Liu, F.; Jiang, P. The influence of the interface between mica and epoxy matrix on properties of epoxy-based dielectric materials with high thermal conductivity and low dielectric loss. *Rsc Adv.* **2016**, *6*, 83163–83174. [CrossRef]

35. Guan, Y.; Lu, H.; Yin, C.; Xue, Y.; Jiang, Y.; Kang, Y.; He, L.; Heiskanen, J. Vegetation response to climate zone dynamics and its impacts on surface soil water content and albedo in China. *Sci. Total Environ.* **2020**, *747*, 141537. [CrossRef] [PubMed]

36. Tan, X.; Wu, J.; Huang, J.; Wu, M.; Zeng, W. Design of a new TDR probe to measure water content and electrical conductivity in highly saline soils. *J. Soils Sediments* **2018**, *18*, 1087–1099. [CrossRef]

37. Kargas, G.; Soulis, K.X. Performance evaluation of a recently developed soil water content, dielectric permittivity, and bulk electrical conductivity electromagnetic sensor. *Agric. Water Manag.* **2019**, *213*, 568–579. [CrossRef]

38. Xu, X.; Zhang, W.; Wang, Y. Measuring and modeling the dielectric constant of soil during freezing and thawing processes: An application on silty clay. *Acta Geotech.* **2022**, *17*, 3867–3886. [CrossRef]

39. Hernandez-Soriano, M.C.; Jimenez-Lopez, J.C. Effects of soil water content and organic matter addition on the speciation and bioavailability of heavy metals. *Sci. Total Environ.* **2012**, *423*, 55–61. [CrossRef] [PubMed]

40. Kabir, H.; Khan, M.J.; Brodie, G.; Gupta, D.; Pang, A.; Jacob, M.V.; Antunes, E. Measurement and modelling of soil dielectric properties as a function of soil class and moisture content. *J. Microw. Power Electromagn. Energy* **2020**, *54*, 3–18. [CrossRef]

41. Topp, G.C.; Davis, J.L.; Annan, A.P. Electromagnetic determination of soil water content: Measurements in coaxial transmission lines. *Water Resour. Res.* **1980**, *16*, 574–582. [CrossRef]

42. He, H.; Dyck, M.; Zhao, Y.; Si, B.; Jin, H.; Zhang, T.; Lv, J.; Wang, J. Evaluation of five composite dielectric mixing models for understanding relationships between effective permittivity and unfrozen water content. *Cold Reg. Sci. Technol.* **2016**, *130*, 33–42. [CrossRef]

43. Pan, X.; Han, Y.; Chun, K.P.; Zhang, J.; Ma, D.; Gao, H. On the laboratory calibration of dielectric permittivity models for agricultural soils: Effect of systematic porosity variation. *Vadose Zone J.* **2021**, *20*, e20096. [CrossRef]

44. Chen, Y.P.; Or, D. Geometrical factors and interfacial processes affecting complex dielectric permittivity of partially saturated porous media. *Water Resour. Res.* **2006**, *42*, W06423. [CrossRef]

45. Majcher, J.; Kafarski, M.; Wilczek, A.; Woszczyk, A.; Szypłowska, A.; Lewandowski, A.; Szerement, J.; Skierucha, W. Application of a Monopole Antenna Probe with an Optimized Flange Diameter for TDR Soil Moisture Measurement. *Sensors* **2020**, *20*, 2374. [CrossRef] [PubMed]

46. Hardie, M. Review of Novel and Emerging Proximal Soil Moisture Sensors for Use in Agriculture. *Sensors* **2020**, *20*, 6934. [CrossRef] [PubMed]

47. Xu, X.; Wang, H.; Qu, X.; Li, C.; Cai, B.; Peng, G. Study on the dielectric properties and dielectric constant model of laterite. *Front. Earth Sci.* **2022**, *10*, 1035692. [CrossRef]

48. Liao, H.; Dong, H.; Ning, C.; Zhang, J.; Sun, J. A new logarithmic dielectric constant model of soils. *Jpn. Geotech. Soc. Spec. Publ.* **2019**, *7*, 281–286. [CrossRef]

49. Xu, J.; Zhou, G.; Su, S.; Cao, Q.; Tian, Z. The Development of A Rigorous Model for Bathymetric Mapping from Multispectral Satellite-Images. *Remote Sens.* **2022**, *14*, 2495. [CrossRef]

50. Xu, Z.; Li, X.; Li, J.; Xue, Y.; Jiang, S.; Liu, L.; Luo, Q.; Wu, K.; Zhang, N.; Feng, Y.; et al. Characteristics of Source Rocks and Genetic Origins of Natural Gas in Deep Formations, Gudian Depression, Songliao Basin, NE China. *ACS Earth Space Chem.* **2022**, *6*, 1750–1771. [CrossRef]

51. Roth, K.; Schulin, R.; Flühler, H.; Attinger, W. Calibration of time domain reflectometry for water content measurement using a composite dielectric approach. *Water Resour. Res.* **1990**, *26*, 2267–2273. [CrossRef]

52. Savin, I.V.; Muzalevskiy, K.V. Dielectric Model for Thawed Organic Soils at Frequency of 435 MHz. *IEEE Geosci. Remote Sens. Lett.* **2021**, *18*, 218–221. [CrossRef]

53. Bogena, H.R.; Huisman, J.A.; Schilling, B.; Weuthen, A.; Vereecken, H. Effective Calibration of Low-Cost Soil Water Content Sensors. *Sensors* **2017**, *17*, 208. [CrossRef]

54. Kibirige, D.; Dobos, E. Off-Site Calibration Approach of EnviroScan Capacitance Probe to Assist Operational Field Applications. *Water* **2021**, *13*, 837. [CrossRef]

55. Huan, Z.; Wang, H.; Li, C.; Wan, C. The soil moisture sensor based on soil dielectric property. *Pers. Ubiquitous Comput.* **2017**, *21*, 67–74. [CrossRef]

56. Bianchi, F.; Chiappini, M.; Giordano, R. Formation, diffusion and distribution of leachate: Integrated mathematical models of SIGLOD project. *Quad. Di Geofis.* **2015**, *128*, 1–30.

57. Wang, J.R. The dielectric properties of soil-water mixtures at microwave frequencies. *Radio Sci.* **1980**, *15*, 977–985. [CrossRef]

58. Park, C.-H.; Behrendt, A.; LeDrew, E.; Wulfmeyer, V. New Approach for Calculating the Effective Dielectric Constant of the Moist Soil for Microwaves. *Remote Sens.* **2017**, *9*, 732. [CrossRef]

59. Wang, J.R.; Schmugge, T.J. An Empirical Model for the Complex Dielectric Permittivity of Soils as a Function of Water Content. *IEEE Trans. Geosci. Remote Sens.* **1980**, *GE-18*, 288–295. [CrossRef]

60. Malicki, M.A.; Plagge, R.; Roth, C.H. Improving the calibration of dielectric TDR soil moisture determination taking into account the solid soil. *Eur. J. Soil Sci.* **1996**, *47*, 357–366. [CrossRef]

61. Robinson, D.A.; Jones, S.B.; Blonquist, J.M.; Friedman, S.P. A Physically Derived Water Content/Permittivity Calibration Model for Coarse-Textured, Layered Soils. *Soil Sci. Soc. Am. J.* **2005**, *69*, 1372–1378. [CrossRef]

62. Gardner, C.M.K.; Dean, T.J.; Cooper, J.D. Soil Water Content Measurement with a High-Frequency Capacitance Sensor. *J. Agric. Eng. Res.* **2018**, *71*, 395–403. [CrossRef]

63. Szerement, J.; Woszczyk, A.; Szypłowska, A.; Kafarski, M.; Lewandowski, A.; Wilczek, A.; Skierucha, W. A Seven-Rod Dielectric Sensor for Determination of Soil Moisture in Well-Defined Sample Volumes. *Sensors* **2019**, *19*, 1646. [CrossRef]

64. Moshayedi, A.J.; Sohail Khan, A.; Hu, J.; Nawaz, A.; Zhu, J. E-Nose-Driven Advancements in Ammonia Gas Detection: A Comprehensive Review from Traditional to Cutting-Edge Systems in Indoor to Outdoor Agriculture. *Sustainability* **2023**, *15*, 11601. [CrossRef]

65. Wojciech, S. Time Domain Reflectometry: Temperature-dependent Measurements of Soil Dielectric Permittivity. In *Electromagnetic Waves*; Vitaliy, Z., Ed.; IntechOpen: Rijeka, Croatia, 2011.

66. Or, D.; Wraith, J.M. Temperature effects on soil bulk dielectric permittivity measured by time domain reflectometry: A physical model. *Water Resour. Res.* **1999**, *35*, 371–383. [CrossRef]

67. Loewer, M.; Günther, T.; Igel, J.; Kruschwitz, S.; Martin, T.; Wagner, N. Ultra-broad-band electrical spectroscopy of soils and sediments—A combined permittivity and conductivity model. *Geophys. J. Int.* **2017**, *210*, 1360–1373. [CrossRef]

68. He, M.-Y.; Dong, J.-B.; Jin, Z.; Liu, C.-Y.; Xiao, J.; Zhang, F.; Sun, H.; Zhao, Z.-Q.; Gou, L.-F.; Liu, W.-G.; et al. Pedogenic processes in loess-paleosol sediments: Clues from Li isotopes of leachate in Luochuan loess. *Geochim. Et Cosmochim. Acta* **2021**, *299*, 151–162. [CrossRef]

69. Vaz, C.M.P.; Jones, S.; Meding, M.; Tuller, M. Evaluation of standard calibration functions for eight electromagnetic soil moisture sensors. *Vadose Zone J.* **2013**, *12*, 1–16. [CrossRef]

70. Adla, S.; Rai, N.K.; Karumanchi, S.H.; Tripathi, S.; Disse, M.; Pande, S. Laboratory Calibration and Performance Evaluation of Low-Cost Capacitive and Very Low-Cost Resistive Soil Moisture Sensors. *Sensors* **2020**, *20*, 363. [CrossRef] [PubMed]

71. Szerement, J.; Saito, H.; Furuhata, K.; Yagihara, S.; Szypłowska, A.; Lewandowski, A.; Kafarski, M.; Wilczek, A.; Majcher, J.; Woszczyk, A.; et al. Dielectric Properties of Glass Beads with Talc as a Reference Material for Calibration and Verification of Dielectric Methods and Devices for Measuring Soil Moisture. *Materials* **2020**, *13*, 1968. [CrossRef] [PubMed]

72. Qi, J.L.; Ma, W. State-of-art of research on mechanical properties of frozen soils. *Rock Soil Mech.* **2010**, *31*, 133–143.

73. Wan, X.; Lai, Y.; Wang, C. Experimental study on the freezing temperatures of saline silty soils. *Permafr. Periglac. Process.* **2015**, *26*, 175–187. [CrossRef]

74. Torres-Rua, A.F.; Ticlavilca, A.M.; Bachour, R.; McKee, M. Estimation of Surface Soil Moisture in Irrigated Lands by Assimilation of Landsat Vegetation Indices, Surface Energy Balance Products, and Relevance Vector Machines. *Water* **2016**, *8*, 167. [CrossRef]

75. Huang, J.; Gómez-Dans, J.L.; Huang, H.; Ma, H.; Wu, Q.; Lewis, P.E.; Liang, S.; Chen, Z.; Xue, J.-H.; Wu, Y.; et al. Assimilation of remote sensing into crop growth models: Current status and perspectives. *Agric. For. Meteorol.* **2019**, *276–277*, 107609. [CrossRef]

76. Stellini, J.; Farrugia, L.; Farhat, I.; Bonello, J.; Persico, R.; Sacco, A.; Spiteri, K.; Sammut, C.V. Broadband Measurements of Soil Complex Permittivity. *Sensors* **2023**, *23*, 5357. [CrossRef]

77. Yao, X.; Yu, X.; Wang, L.; Zeng, Y.; Mao, L.; Liu, S.; Xie, H.; He, G.; Huang, Z.; Liu, Z. Preparation of cinnamic hydroxamic acid collector and study on flotation characteristics and mechanism of scheelite. *Int. J. Min. Sci. Technol.* **2023**, *33*, 773–781. [CrossRef]

78. Lu, Q.; Liu, K.; Zeng, Z.; Liu, S.; Li, R.; Xia, L.; Guo, S.; Li, Z. Estimation of the Soil Water Content Using the Early Time Signal of Ground-Penetrating Radar in Heterogeneous Soil. *Remote Sens.* **2023**, *15*, 3026. [CrossRef]
79. Zhang, T.; Song, B.; Han, G.; Zhao, H.; Hu, Q.; Zhao, Y.; Liu, H. Effects of coastal wetland reclamation on soil organic carbon, total nitrogen, and total phosphorus in China: A meta-analysis. *Land Degrad. Dev.* **2023**, *34*, 3340–3349. [CrossRef]
80. Mohanty, B.P.; Cosh, M.H.; Lakshmi, V.; Montzka, C. Soil moisture remote sensing: State-of-the-science. *Vadose Zone J.* **2017**, *16*, 1–9. [CrossRef]
81. Lakshmi, V. Remote Sensing of Soil Moisture. *ISRN Soil Sci.* **2013**, *2013*, 424178. [CrossRef]
82. Araya, S.N.; Fryjoff-Hung, A.; Anderson, A.; Viers, J.H.; Ghezzehei, T.A. Advances in soil moisture retrieval from multispectral remote sensing using unoccupied aircraft systems and machine learning techniques. *Hydrol. Earth Syst. Sci.* **2021**, *25*, 2739–2758. [CrossRef]
83. Babaeian, E.; Sadeghi, M.; Jones, S.B.; Montzka, C.; Vereecken, H.; Tuller, M. Ground, Proximal, and Satellite Remote Sensing of Soil Moisture. *Rev. Geophys.* **2019**, *57*, 530–616. [CrossRef]
84. Yin, L.; Wang, L.; Li, T.; Lu, S.; Yin, Z.; Liu, X.; Li, X.; Zheng, W. U-Net-STN: A Novel End-to-End Lake Boundary Prediction Model. *Land* **2023**, *12*, 1602. [CrossRef]
85. Jia, B.; Zhou, G. Estimation of global karst carbon sink from 1950s to 2050s using response surface methodology. *Geo-Spat. Spat. Spat. Inf. Sci.* **2023**, 1–18. [CrossRef]
86. Yin, L.; Wang, L.; Li, T.; Lu, S.; Tian, J.; Yin, Z.; Li, X.; Zheng, W. U-Net-LSTM: Time Series-Enhanced Lake Boundary Prediction Model. *Land* **2023**, *12*, 1859. [CrossRef]
87. Alexandridis, T.K.; Cherif, I.; Bilas, G.; Almeida, W.G.; Hartanto, I.M.; Van Andel, S.J.; Araujo, A. Spatial and Temporal Distribution of Soil Moisture at the Catchment Scale Using Remotely-Sensed Energy Fluxes. *Water* **2016**, *8*, 32. [CrossRef]
88. Koch, F.; Schlenz, F.; Prasch, M.; Appel, F.; Ruf, T.; Mauser, W. Soil Moisture Retrieval Based on GPS Signal Strength Attenuation. *Water* **2016**, *8*, 276. [CrossRef]
89. Li, Z.; Zeng, Z.; Xiong, H.; Lu, Q.; An, B.; Yan, J.; Li, R.; Xia, L.; Wang, H.; Liu, K. Study on Rapid Inversion of Soil Water Content from Ground-Penetrating Radar Data Based on Deep Learning. *Remote Sens.* **2023**, *15*, 1906. [CrossRef]
90. Qiu, S.; Yang, H.; Zhang, S.; Huang, S.; Zhao, S.; Xu, X.; He, P.; Zhou, W.; Zhao, Y.; Yan, N.; et al. Carbon storage in an arable soil combining field measurements, aggregate turnover modeling and climate scenarios. *CATENA* **2023**, *220*, 106708. [CrossRef]
91. Ozgur, M. Development and validation of a degree of saturation prediction model using time domain reflectometry for compaction control. *Transp. Geotech.* **2023**, *42*, 101062. [CrossRef]
92. González-Teruel, J.D.; Jones, S.B.; Soto-Valles, F.; Torres-Sánchez, R.; Lebron, I.; Friedman, S.P.; Robinson, D.A. Dielectric Spectroscopy and Application of Mixing Models Describing Dielectric Dispersion in Clay Minerals and Clayey Soils. *Sensors* **2020**, *20*, 6678. [CrossRef] [PubMed]
93. Dyck, M.; Miyamoto, T.; Iwata, Y.; Kameyama, K. Bound Water, Phase Configuration, and Dielectric Damping Effects on TDR-Measured Apparent Permittivity. *Vadose Zone J.* **2019**, *18*, 190027. [CrossRef]
94. He, H.; Flerchinger, G.N.; Kojima, Y.; Dyck, M.; Lv, J. A review and evaluation of 39 thermal conductivity models for frozen soils. *Geoderma* **2021**, *382*, 114694. [CrossRef]
95. He, H.; Dyck, M. Application of Multiphase Dielectric Mixing Models for Understanding the Effective Dielectric Permittivity of Frozen Soils. *Vadose Zone J.* **2013**, *12*, 1–22. [CrossRef]
96. Greco, R.; Guida, A. Field measurements of topsoil moisture profiles by vertical TDR probes. *J. Hydrol.* **2018**, *348*, 442–451. [CrossRef]
97. Regalado, C.M. A physical interpretation of logarithmic TDR calibration equations of volcanic soils and their solid fraction permittivity based on Lichtenecker's mixing formulae. *Geoderma* **2014**, *123*, 41–50. [CrossRef]
98. Gnatowski, T.; Szatyłowicz, J.; Pawluśkiewicz, B.; Oleszczuk, R.; Janicka, M.; Papierowska, E.; Szejba, D. Field Calibration of TDR to Assess the Soil Moisture of Drained Peatland Surface Layers. *Water* **2018**, *10*, 1842. [CrossRef]
99. Pepin, S.; Livingston, N.J.; Hook, W.R. Temperature-Dependent Measurement Errors in Time Domain Reflectometry Determinations of Soil Water. *Soil Sci. Soc. Am. J.* **2015**, *59*, 38–43. [CrossRef]
100. Cui, F.; Ni, J.; Du, Y.; Zhao, Y.; Zhou, Y. Soil water content estimation using ground penetrating radar data via group intelligence optimization algorithms: An application in the Northern Shaanxi Coal Mining Area. *Energy Explor. Exploit.* **2020**, *39*, 318–335. [CrossRef]
101. Mukhlisin, M.; Saputra, A.; Taha, M. A New Model of Dielectric Analysis for Measurement Soil Moisture Water Content. *J. Eng. Sci. Technol.* **2013**, *13*, 2910.
102. Amankwah, S.K.; Ireson, A.M.; Brannen, R. An improved model and field calibration technique for measuring liquid water content in unfrozen and frozen soils with dielectric probes. *Vadose Zone J.* **2022**, *21*, e20225. [CrossRef]
103. Xu, J.; Logsdon, S.; Ma, X.; Horton, R.; Han, W.; Zhao, Y. Measurement of Soil Water Content with Dielectric Dispersion Frequency. *Soil Sci. Soc. Am. J.* **2014**, *78*, 1500. [CrossRef]
104. Inaudi, D.; Glisic, B. Distributed fiber-optic sensing for long-range monitoring of pipelines. In Proceedings of the 3rd International Conference on Structural Health Monitoring of Intelligent Infrastructure, Vancouver, BC, Canada, 13–16 November 2007; pp. 1–8.
105. Peng, J.; Loew, A. Recent Advances in Soil Moisture Estimation from Remote Sensing. *Water* **2017**, *9*, 530. [CrossRef]
106. Satoh, Y.; Kakiuchi, H. Calibration method to address influences of temperature and electrical conductivity for a low-cost soil water content sensor in the agricultural field. *Agric. Water Manag.* **2021**, *255*, 107015. [CrossRef]

107. Peng, W.; Lu, Y.; Wang, M.; Ren, T.; Horton, R. Determining water content and bulk density: The heat-pulse method outperforms the thermo-TDR method in high-salinity soils. *Geoderma* **2022**, *407*, 115564. [CrossRef]

108. Lu, Y.; Song, W.; Lu, J.; Wang, X.; Tan, Y. An Examination of Soil Moisture Estimation Using Ground Penetrating Radar in Desert Steppe. *Water* **2017**, *9*, 521. [CrossRef]

109. Zhou, L.; Yu, D.; Wang, X.; Wang, X.; Zhang, H. Determination of top soil water content based on high-frequency ground penetrating radar. *Acta Pedol. Sin.* **2016**, *53*, 621–626.

110. Dai, H.; Liu, Y.; Guadagnini, A.; Yuan, S.; Yang, J.; Ye, M. Comparative Assessment of Two Global Sensitivity Approaches Considering Model and Parameter Uncertainty. *Water Resour. Res.* **2024**, *60*, e2023WR036096. [CrossRef]

111. Zhao, Y.; Ding, Z.; Shen, C.; Chen, Y. Interfacial microstructure and properties of aluminum–magnesium AZ31B multi-pass friction stir processed composite plate. *Mater. Des.* **2016**, *94*, 240–252. [CrossRef]

112. Ju, Z.; Liu, X.; Ren, T.; Hu, C. Measuring soil water content with time domain reflectometry: An improved calibration considering soil bulk density. *Soil Sci.* **2010**, *175*, 469–473. [CrossRef]

113. Whalley, W.R.; Leeds-Harrison, P.B.; Whitmore, A.P.; Sarker, P.K. Effect of aggregate size on the water content estimated with time domain reflectance [TDR]. *Int. Agrophys.* **2014**, *18*, 181–187.

114. Skierucha, W. Accuracy of soil moisture measurement by TDR technique. *Int. Agrophys.* **2020**, *14*, 417–426.

115. Siddiqui, S.I.; Drnevich, V.P. *A New Method of Measuring Density and Moisture Content of Soil Using the Technique of Time Domain Reflectometry*; Joint Highway Research Project; Purdue University: Lafayette, IN, USA, 1995.

116. Friedman, S.P. Statistical Mixing Model for the Apparent Dielectric Constant of Unsaturated Porous Media. *Soil Sci. Soc. Am. J.* **1997**, *61*, 742–745. [CrossRef]

117. Peplinski, N.R.; Ulaby, F.T.; Dobson, M.C. Dielectric Properties of Soils in the 0.3–1.3-GHz Range. *IEEE Trans. Geosci. Remote Sens.* **1995**, *33*, 803–807. [CrossRef]

118. Zhao, Y.; Ling, D.-s.; Wang, Y.-l.; Huang, B.; Wang, H.-l. Study on a calibration equation for soil water content in field tests using time domain reflectometry. *J. Zhejiang Univ. SCIENCE A* **2016**, *17*, 240–252. [CrossRef]

119. Liu, X.; Chen, J.; Cui, X.; Liu, Q.; Cao, X.; Chen, X. Measurement of soil water content using ground-penetrating radar: A review of current methods. *Int. J. Digit. Earth* **2019**, *12*, 95–118. [CrossRef]

120. Koyama, C.N.; Liu, H.; Takahashi, K.; Shimada, M.; Watanabe, M.; Khuut, T.; Sato, M. In-Situ Measurement of Soil Permittivity at Various Depths for the Calibration and Validation of Low-Frequency SAR Soil Moisture Models by Using GPR. *Remote Sens.* **2017**, *9*, 580. [CrossRef]

121. Mukhlisin, M.; Astuti, H.W.; Wardihani, E.D.; Matlan, S.J. Techniques for ground-based soil moisture measurement: A detailed overview. *Arab. J. Geosci.* **2021**, *14*, 2032. [CrossRef]

122. Comite, D.; Galli, A.; Lauro, S.E.; Mattei, E.; Pettinelli, E. Analysis of GPR early-time signal features for the evaluation of soil permittivity through numerical and experimental surveys. *IEEE J. Sel. Top. Appl. Earth Obs. Remote Sens.* **2015**, *9*, 178–187. [CrossRef]

123. Busch, S.; Van der Kruk, J.; Vereecken, H. Improved characterization of fine-texture soils using on-ground GPR full-waveform inversion. *IEEE Trans. Geosci. Remote Sens.* **2013**, *52*, 3947–3958. [CrossRef]

124. Novák, V.; Hlaváčiková, H. Soil-Water Content and Its Measurement. In *Applied Soil Hydrology*; Novák, V., Hlaváčiková, H., Eds.; Springer International Publishing: Cham, Switzerland, 2019; pp. 49–61.

125. He, H.; Turner, N.C.; Aogu, K.; Dyck, M.; Feng, H.; Si, B.; Wang, J.; Lv, J. Time and frequency domain reflectometry for the measurement of tree stem water content: A review, evaluation, and future perspectives. *Agric. For. Meteorol.* **2021**, *306*, 108442. [CrossRef]

126. Zhu, Y.; Irmak, S.; Jhala, A.; Vuran, M.; Diotto, A. Time-domain and Frequency-domain Reflectometry Type Soil Moisture Sensor Performance and Soil Temperature Effects in Fine- and Coarse-textured Soils. *Appl. Eng. Agric.* **2019**, *35*, 117–134. [CrossRef]

127. De Vos, B.; Cools, N.; Verstraeten, A.; Neirynck, J. Accurate Measurements of Forest Soil Water Content Using FDR Sensors Require Empirical In Situ (Re)Calibration. *Appl. Sci.* **2021**, *11*, 11620. [CrossRef]

128. Lü, H.B.; Jiang, W.Y.; Zhao, Y.L.; Zeng, Z.T. Relationship between volumetric water content and effective dielectric permittivity of Nanning expansive soil. *Rock Soil Mech.* **2016**, *37*, 2145–2150.

129. Orangi, A.; Narsilio, G.A.; Ryu, D. A Laboratory Study on Non-Invasive Soil Water Content Estimation Using Capacitive Based Sensors. *Sensors* **2019**, *19*, 651. [CrossRef] [PubMed]

130. Lv, L.; Liao, K.; Lai, X.; Zhu, Q.; Zhou, S. Hillslope soil moisture temporal stability under two contrasting land use types during different time periods. *Environ. Earth Sci.* **2016**, *75*, 560. [CrossRef]

131. Bajno, D.; Bednarz, L.; Matkowski, Z.; Raszczuk, K. Monitoring of Thermal and Moisture Processes in Various Types of External Historical Walls. *Materials* **2020**, *13*, 505. [CrossRef] [PubMed]

132. Dettmann, U.; Bechtold, M. Evaluating Commercial Moisture Probes in Reference Solutions Covering Mineral to Peat Soil Conditions. *Vadose Zone J.* **2018**, *17*, 170208. [CrossRef]

133. Susha Lekshmi, S.U.; Singh, D.N.; Shojaei Baghini, M. A critical review of soil moisture measurement. *Measurement* **2014**, *54*, 92–105.

134. Romanov, A.N. Influence of Water Content and Temperature on the Dielectric and Radio-Emitting Properties of the Salt Crust of Puffy Solonchak. *Eurasian Soil Sci.* **2019**, *52*, 171–179. [CrossRef]

135. Xu, X.; Zhang, W.; Fan, C.; Li, G. Effects of temperature, dry density and water content on the thermal conductivity of Genhe silty clay. *Results Phys.* **2020**, *16*, 102830. [CrossRef]

136. Yan, G.; Bore, T.; Bhuyan, H.; Schlaeger, S.; Scheuermann, A. The Technical Challenges for Applying Unsaturated Soil Sensors to Conduct Laboratory-Scale Seepage Experiments. *Sensors* **2022**, *22*, 3724. [CrossRef]

137. Yu, J.; Zhu, Y.; Yao, W.; Liu, X.; Ren, C.; Cai, Y.; Tang, X. Stress relaxation behaviour of marble under cyclic weak disturbance and confining pressures. *Measurement* **2021**, *182*, 109777. [CrossRef]

138. Ren, C.; Yu, J.; Liu, S.; Yao, W.; Zhu, Y.; Liu, X. A Plastic Strain-Induced Damage Model of Porous Rock Suitable for Different Stress Paths. *Rock Mech. Rock Eng.* **2022**, *55*, 1887–1906. [CrossRef]

139. Xu, L.L.; Gao, C.H.; Wang, J.M. Evaluation and analysis of TDR calibration curves for soil water content measurement. *J. Glaciol. Geocryol.* **2020**, *42*, 265–275.

140. He, H.; Aogu, K.; Li, M.; Xu, J.; Sheng, W.; Jones, S.B.; González-Teruel, J.D.; Robinson, D.A.; Horton, R.; Bristow, K.; et al. A review of time domain reflectometry (TDR) applications in porous media. In *Advances in Agronomy*; Sparks, D.L., Ed.; Academic Press: Cambridge, MA, USA, 2021; Volume 168, pp. 83–155.

141. Underwood, T.R.; Bourg, I.C. Dielectric Properties of Water in Charged Nanopores. *J. Phys. Chem. B* **2022**, *126*, 2688–2698. [CrossRef] [PubMed]

142. Mohan, V.B.; Jayaraman, K.; Bhattacharyya, D. Brunauer–Emmett–Teller (BET) specific surface area analysis of different graphene materials: A comparison to their structural regularity and electrical properties. *Solid State Commun.* **2020**, *320*, 114004. [CrossRef]

143. Zhao, Y.; Wang, H.; Song, B.; Xue, P.; Zhang, W.; Peth, S.; Lee Hill, R.; Horn, R. Characterizing uncertainty in process-based hydraulic modeling, exemplified in a semiarid Inner Mongolia steppe. *Geoderma* **2023**, *440*, 116713. [CrossRef]

144. Abdullah, N.H.H.; Kuan, N.W.; Ibrahim, A.; Ismail, B.N.; Majid, M.R.A.; Ramli, R.; Mansor, N.S. *Determination of Soil Water Content Using Time Domain Reflectometer (TDR) for Clayey Soil*; Advances in Civil Engineering and Science Technology; AIP Publishing: Melville, NY, USA, 2018.

145. Singh, J.; Lo, T.; Rudnick, D.R.; Dorr, T.J.; Burr, C.A.; Werle, R.; Shaver, T.M.; Muñoz-Arriola, F. Performance assessment of factory and field calibrations for electromagnetic sensors in a loam soil. *Agric. Water Manag.* **2018**, *196*, 87–98. [CrossRef]